Photolyase: Its Damaged DNA Substrate and Amino Acid Radical Formation During Photorepair

Eldon Kenneth Hurley Jr.

Thesis submitted to the faculty of the Virginia Polytechnic Institute and State University
in partial fulfillment of the requirements for the degree of

Master of Science
in
Biochemistry

Sunyoung Kim, Chair
David R. Bevan
Peter J. Kennelly
John B. Phillips

January 6th, 2005
Blacksburg, VA

Keywords: photolyase, DNA repair, thymine dimer, amino acid radical

Photolyase: Its Damaged DNA Substrate and Amino Acid Radical Formation During Photorepair

Eldon Kenneth Hurley Jr.

ABSTRACT

Ultraviolet light damages genomic material by inducing the formation of covalent bonds between adjacent pyrimidines. *Cis-syn* cyclobutane pyrimidine dimers (CPD) constitute the most abundant primary lesion in DNA. Photolyase, a light-activated enzyme, catalytically repairs these lesions. Although many steps in the photolyase-mediated repair process have been mapped, details of the mechanism remain cryptic. Difference FT-IR spectroscopy was employed to obtain new mechanistic information about photorepair. Purified oligonucleotides, containing a central diuracil, dithymidine, or cyclobutane thymidine dimer, were monitored using vibrational methods. Construction of difference infrared data between undamaged and damaged DNA permitted examination of nucleic acid changes upon formation of the CPD lesion; these experiments indicated that C=O and C-H frequencies can be used as markers for DNA damage. Furthermore, in purified photolyase containing isotopically-labeled aromatic amino acids, we observed that tryptophan residues in photolyase underwent structural changes during photorepair. These data indicate that electron transfer during DNA repair occurs through-bond, and that redox-active, aromatic residues form the pathway for electron transfer.

ACKNOWLEDGEMENTS

For their contributions to my education, scientific understanding, and scientific career, I would like to acknowledge the following people:

My advisor, Sunyoung Kim, first for the opportunity to start my scientific career in her lab as a technician, and second for encouraging me to work toward an advanced degree.

My thesis committee, David Bevan, Peter Kennelly, and John Phillips for their patience, understanding, and insight.

W. H. Velander and the members of his laboratory, for introducing me to scientific research.

The past and present members of the Kim Lab, for the fun, effort, and support provided over the years.

My inner-circle: Amanda, Graham, Jory, Joe, Craig, Laura, Tina, Kevin, Matt, Rob, Lauren, and Clark, for being themselves.

And finally, my family, for the love, support, and general encouragement they have always provided.

TABLE OF CONTENTS

FIGURES

CHAPTER I

CHAPTER II

CHAPTER III

TABLES

CHAPTER II

CHAPTER III

ABBREVIATIONS

8merTT	GAATTAAG
8merTTCPD	GAAT<>TAAG
8merUU	GAAUUAAG
β-ME	β-mercaptoethanol
CPD	cyclobutane pyrimidine dimer
DNA	deoxyribonucleic acid
DTT	dithiothreitol
EDTA	ethylenediaminetetraacetic acid
FT-IR spectroscopy	Fourier Transform-infrared spectroscopy
HEPES	4-(2-hydroylethyl)piperazine-1-ethanesulfonic acid
HPLC	high performance liquid chromatography
IPTG	isopropylβ-D-1-thiogalactopyranoside
LB	Luria-Bertani medium
MALDI-TOF	Matrix-assisted laser desorption ionization time-of-flight mass spectrometry
MCT	mercury cadmium telluride
phrA	photolyase
PVDF	polyvinylidene fluoride
ssDNA	single stranded deoxyribonucleic acid
thymine	5-methyl-2,4,-dioxopyrimidine
thymidine	1-2(-Deoxy-β-D-ribofuranosyl)thymine
Tris	Tris[hydroxymethyl]aminomethane
uracil	2,4,-dioxopyrimidine
UV	ultraviolet
Vis	visible

CHAPTER I

Introduction and Literature Review

OVERVIEW OF THESIS

Photoreactivation is the recovery of organisms, injured by ultraviolet (UV) light, by the application of visible light (*1*). Detection and characterization of this phenomenon are the foundation for the field of research dedicated to understanding DNA damage and DNA repair [reviewed in (*2*)]. The term *photoreactivation* has been replaced in contemporary literature by the term *photorepair*, which more adequately describes the biochemical process involved (*3*). Using vibrational spectroscopy, we detail the molecular changes that occur in both substrate and enzyme during the photorepair process. The specific objectives of this thesis were:

Objective I. To characterize the vibrational signatures that indicate the presence of a cyclobutane pyrimidine dimer in oligonucleotides.

Objective II. To determine if tryptophan is a participant in the electron transfer event that leads to DNA repair by *E. coli* photolyase.

The principal consequence of this work is to establish and extend the use of vibrational spectroscopy from the study of small chemical models to more complex biomolecules, with the purpose of contributing to the understanding of the photorepair process.

LITERATURE REVIEW

1.1 The Photoreactivation Phenomenon

Photoreactivation was first described in 1949. When working with *S. griseus,* Alfred Kelner observed that cultures placed near the glass front of an incubation bath remained viable after UV irradiation (*1*). In contrast, cultures placed toward the back of

the incubator were killed by the same UV irradiation. The ability of cells to regain viability upon treatment with visible light was supported by the work of Dulbecco (*4*), who found that bacteria could restore the viability of irradiated bacteriophage upon illumination. Although the concept of organismal inactivation by UV light had been described as early as 1892 (*5*), these reports were the first to describe and identify the light-driven photoreactivation phenomenon.

Although the cellular target of UV damage and reactivation mechanism were not known, the general parameters of UV-damage and photoreactivation were determined. Cell damage and death required light from the UV-blue region of the spectrum: wavelengths less than 300 nm could inhibit or stop cell growth, with light between 265 and 254 nm having the greatest impact (*6*). The narrow range of wavelengths sufficient to affect cell death implied that a specific chromophore absorbed the energy (*6*). Photoreactivation was also observed to be wavelength dependent, but longer wavelengths are required to facilitate repair, suggesting an altogether different chromophore, distinct from that utilized in damage (*7*). These discoveries supported an earlier postulate that photoreactivation was an enzymatic process (*4*).

When DNA was established as the source of heredity (*8*), and that the genetic function is dependent on DNA sequence and structure (*9, 10*), the target of UV irradiation was argued to be genomic material. It was observed that sufficiently high doses of irradiation could affect all the components of nucleic acids, but the pyrimidine bases were most susceptible, thymidine in particular (*11*). Of note is the fact that the most damaging region of the UV spectrum is where the DNA bases absorb the most strongly (*12*).

1.2 DNA Damage

The first evidence (*11*) of the CPD lesion in DNA came from examination of thymine, the UV absorbing portion of the thymidine molecule. Irradiation of thymine in water had little effect on the molecule, but irradiation of dilute solutions of thymine (~3.2 mM) in ice led to a loss in UV absorbance. By studying the photoproduct formed from frozen thymine solutions, it was determined that a thymine dimer formed via a cyclobutane bridge between the C5 and C6 atoms (*13*). The frozen state was required to mimic the highly ordered structure of the DNA molecule and drive the thymine molecules together in the proper orientation to form a dimer.

Thymine can form four types of cyclobutane dimers: *cis-syn*, *trans-syn*, *cis-anti*, and *trans-anti*, depending upon orientation of the thymine rings to one another, and the position the C5 and C6 groups occupy (Figure 1.1). The first thymine dimer identified was the *trans-syn* dimer, where the thymine bases are rotated 180º with respect to each other and are joined by single bonds from the C5 of one molecule to the C6 of another. Although this was shown to be the solution structure for irradiated thymine (*13*), it was proposed that, in a DNA molecule, the thymine molecules would be oriented with one intra-molecule single bond between the C5 positions and a second between the C6 positions, forming either the *trans-syn* or *cis-syn* isomer. Isolation and purification of the four individual thymine dimers (*14*), identification of the thymine dimer that is formed in DNA (*15*), and determination of the structure by X-ray crystallography (*16*) collectively demonstrated that irradiated DNA contains predominantly the *cis-syn* cyclobutane dimer. It has been found that up to 66% of the thymidine residues become crosslinked when solutions of oligomeric thymidine (poly T) are exposed to UV light. In comparison,

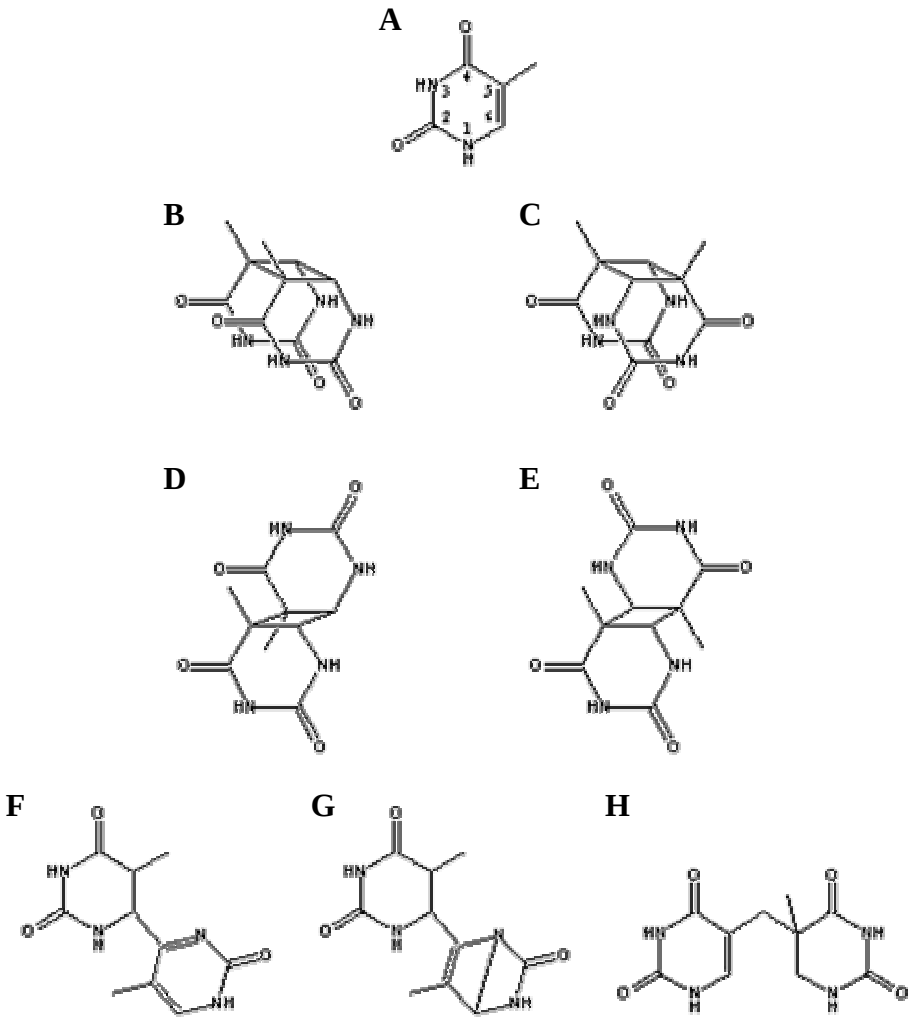

Figure 1.1. Thymine and Thymine Dimers. (A) The ring numbering system for thymine. Cyclobutane pyrimidine dimers can adopt four conformations: (B) *cis-syn*, (C) *trans-syn*, (D) *cis-anti*, and (E) *trans-anti*. Other possible non-cyclobutyl dimers are the (6-4) photoproduct (F) and the Dewar valence isomer of the (6-4) photoproduct (G). Under desiccation conditions the spore photoproduct (H) can be formed.

E. coli DNA under similar conditions has 20% of its total number of the thymidines found in CPDs (*17*).

The pyrimidine bases also can form other types of dimers (Figure 1.1). Instead of being joined by a cyclobutane ring, the two bases can be joined by a single bond from C6 to C4', forming the (6-4) photoproduct. One isomer of the (6-4) photoproduct is the Dewar valence isomer, where N3' is joined to C6' by a single bond. The final known type of pyrimidine dimer occurs in spores, and therefore is referred to as the spore photoproduct. This dimer is generated by the formation of a single bond from the methyl group of a thymine molecule to the C5 of another thymine molecule, with a conversion of the C5=C6 double bond in the second thymine to a single bond. Reference to the (6-4) and spore photoproducts is made because their formation is dependent upon the irradiation conditions, and generally occurs subsequent to CPD formation (*18*). It has been demonstrated that formation of CPD dimers happens almost immediately upon UV irradiation *in vitro* (*19*). The (6-4) photoproducts form much more slowly, hours of irradiation are required to obtain this photoproduct in high yield, with subsequent irradiation with 313 nm light to generate the Dewar valence isomer (*18*). Spore photoproducts require that the pyrimidine molecules be in a dehydrated state and subjected to prolonged, high intensity UV light (*18*). Because of its methylene bridge, the spore photoproduct requires that both molecules of the dimer be thymine. All other dimers can be generated from any combination of thymine, cytosine, and uracil.

Using mammalian cell systems, there is evidence that the (6-4) photoproduct occurs less frequently than CPD type dimers, which make up greater than 80% of the UV induced DNA lesions (*19*). However, the (6-4) photoproducts lead to a higher frequency

of mutation, with (6-4)TT resulting in mutation more often than the (6-4)TC photoproduct (*19*). The CPD lesion formed between two thymines is the least mutagenic, but the higher number of lesions formed increase the chance of an error occurring. It is therefore important that these types of lesions be efficiently and quickly repaired, to prevent cell death and formation of the subsequent photoproducts that tend to be more mutagenic.

Earlier, photoreactivation was stated to be the light-mediated recovery process that occurs following UV insult. Purification of the major UV photoproduct and the photoreactivating enzyme demonstrated that the repair process was catalytic and involved cleavage of the cyclobutane ring between thymine dimers (Figure 1.2). To better describe the enzyme and process taking place, the term photoreactivation was replaced by photorepair, recognizing that it was a light-mediated restoration of proper DNA structure (*3*). In parallel, since the photorepair reaction involves the cleavage of carbon – carbon single bonds, the term photoreactivating enzyme was replaced by photolyase to adequately reflect the reaction catalyzed (*3*).

1.3 Photolyase

Deoxypyrimidine photolyase (EC 4.1.99.3) catalyzes the light driven photorepair reaction (*3, 20*). Although the enzyme has been found in all kingdoms of life, it has not been found in placental animals, such as humans (*21*). Common to all CPD photolyase enzymes is a non-covalently bound cofactor, flavin adenine dinucleotide (FAD). The enzyme may possess a second chromophore, but FAD in the reduced state is the only cofactor required for enzyme function.

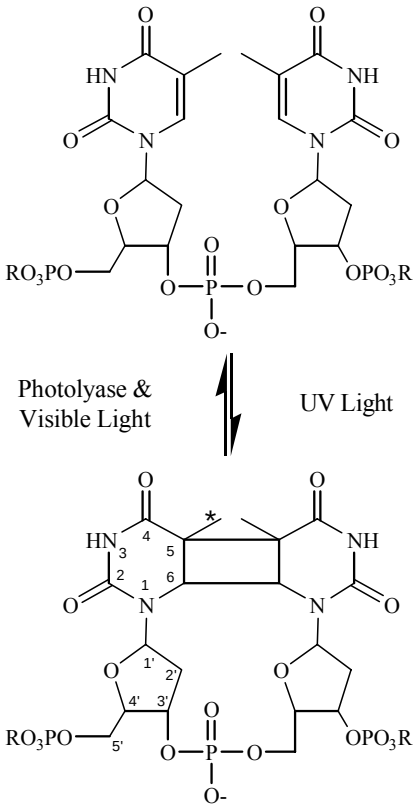

Figure 1.2. DNA Damage and Repair. Adjacent pyrimidines on a DNA strand can dimerize in the presence of UV light to form a cyclobutane pyrimidine dimer. The DNA repair enzyme photolyase catalyzes the reverse reaction in the presence of visible light. The numbering system shown in the lower portion is used throughout the text for both damaged and non damaged DNA. (*) Can be either a hydrogen atom in the case of uridine or CH_3 for thymidine.

Upon purification, the flavin cofactor (Figure 1.3) exists as a neutral radical (*22*) that may be driven to the reduced state by a strong external reductant (*23*) or by a second light-driven intraprotein electron transfer process termed photoactivation (*24*). The enzyme binds to CPD containing double- or single-stranded DNA with high affinity in the presence or absence of light, in either the neutral radical or reduced state (*25*). The repair reaction involves the light-driven one electron transfer from the $FADH^-$ cofactor to the pyrimidine dimer (*26*). Because the reaction requires light, the enzyme-substrate complex is stable in the dark, facilitating biochemical studies.

Initial studies of thymine dimers determined that the molecules were stable under harsh environments, such as high heat or high acid concentrations (*13*). It follows that the mechanism for dimer splitting would require destruction and reformation of the individual pyrimidine rings and require the addition of an electron to drive dimer splitting, since electron abstraction from the dimer was found to be thermodynamically unfavorable (*27*). Fluorescence quenching and molecular modeling calculations (*28*) reveal that splitting of the dimer by electron addition is thermodynamically favorable with $\Delta G = -20$ kcal/mol.

However, the high reduction potential (-2.2 V) of the pyrimidine dimers presents a significant energy barrier to the initiation of the reaction (*28*). A proposed mechanism for pyrimidine dimer splitting (Figure 1.4) starts with the pyrimidine dimer accepting an electron from a donor molecule, and a dimer radical anion is formed. The C5-C5 bond is broken first and a new radical anion intermediate is formed. Following bond rearrangement the electron is ejected from the system, and a neutral di-radical is formed.

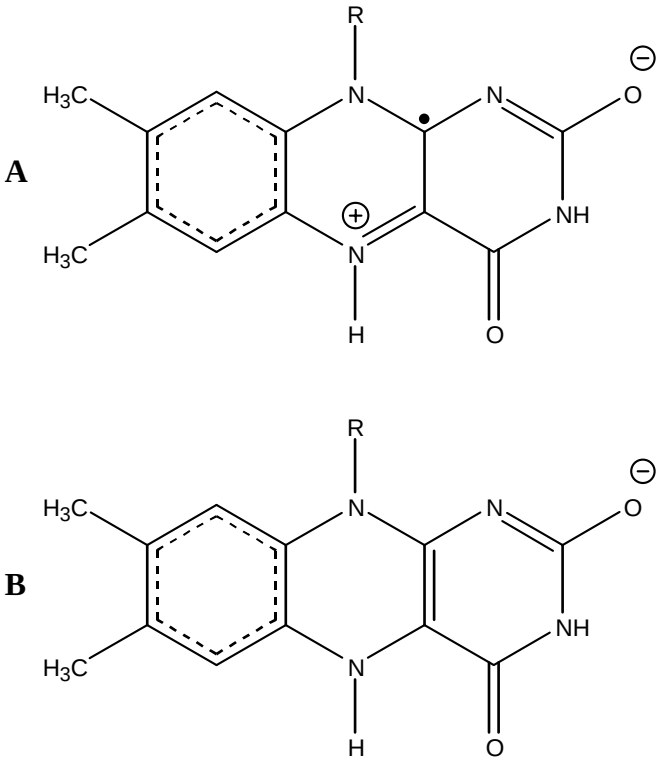

Figure 1.3. Electronic Structure of Isoalloxazine in FADH. Shown in (A) is the neutral radical form of the alloxazine ring of FADH. A one electron reduction induces a bond rearrangement in the structure, generating the (B) reduced form of FADH.

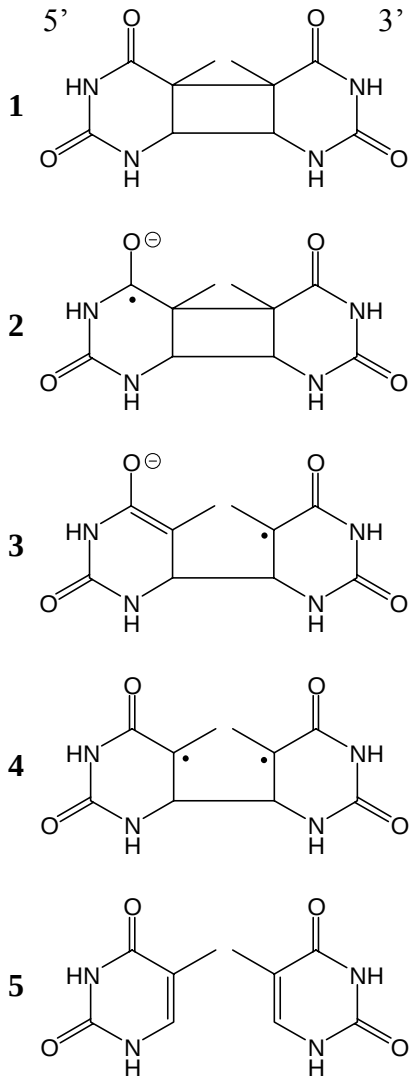

Figure 1.4. Anionic Dimer Splitting Mechanism. Photolyase catalyzes the splitting of a CPD lesion (1) by the addition of an electron to form the pyrimidine-pyrimidine anion (2). The 5'C5-3'C5 single bond is cleaved, and the unpaired electron migrates to the C5 position of the 3' ring. The electron leaves the lesion, generating the di-neutral radical form of the lesion (4). The 5'C6-3'C6 bond is destabilized and cleaved, restoring the thymines to their monomer form. The reaction mechanism and schematic is adapted from Heelis et al (*27*).

The unstable di-radical causes the splitting of the C6-C6 linkage, leaving the repaired pyrimidines.

The activation energy for dimer radical anion formation can be supplied by $FADH^-$. Upon illumination, an electron in $FADH^-$ is excited to the singlet state, with a potential of -2.7 V (*28*). This potential is great enough to donate an electron to the dimer. Experimental evidence has proven that the photorepair mechanism is a one electron transfer event, and that $FADH^-$ is the donor molecule (*29-32*). One major, remaining question in the reaction mechanism in which $FADH^-$ supplies an electron to the dimer is the distance between the two molecules.

The debate over the FAD-dimer distance is fundamental to our understanding of protein mediated electron transfer in photolyase in particular, and in proteins in general. It is incumbent on nature to develop a way for a protein to "gate" electron transfer over short distances, or to facilitate electron transfer over longer distances. The simplest way to prevent the reversal of electron flow, or charge recombination, is to separate the electron donor and acceptor molecules by a large distance. While the Förster model allows *energy* transfer up to 100 Å between metal centers, *electron* transfer through space is limited to a distance of approximately 10 Å (*33*). Electron transfer exceeding a distance of 10 Å has been noted in proteins, demonstrating that the intervening protein matrix can have a profound effect on electron transfer (*34*). It is postulated that long distance transfer or short-distance gating can be accomplished by electron "tunneling" along the peptide backbone or along a chain of redox active cofactors (*33*), both considered as through-bond electron transfer.

A number of studies have tried to validate these models: Does photolyase cradle the cofactor and substrate close enough for permissive electron transfer, or does the protein itself provide a conduit for electron transfer. Photolyase enzymes from *E. coli, T. thermophilus,* and *A. nidulans* have been crystallized in the absence of substrate (*35-37*), and all three structures have been found to be very similar. The enzyme in general consists of an α/β-domain and an α-helical domain that forms the FAD binding domain and catalytic site for the repair of dimers. The FAD cofactor is bound in a U-shaped conformation, unusual for this cofactor (*35-37*), which brings the adenine moiety near the alloxazine ring (Figure 1.5A). A number of molecular modeling studies have used the crystal structure of *E. coli* photolyase to determine the orientation of the substrate in the enzyme (Figure 1.5B). Conflicting results have been obtained, however, because they have shown that the bound substrate may be as close as 3 Å (*38, 39*) or as far 10 Å away from the isoalloxazine ring of the flavin cofactor (*40, 41*).

In contrast to the modeling studies, experimental evidence indicates that the dimer sits approximately 14 Å away from the flavin cofactor (*30*). Only recently have three-dimensional structures of the enzyme substrate complex been reported using *A. nidulans* and *T. thermophilus* photolyase enzymes (*42-44*). The results from these experiments show that in the enzyme-substrate crystal structure, the CPD lesion resides 3.1 Å from the adenine moiety of FAD (*42*), in direct contrast to the NMR solution studies where the CPD is 16 Å from the alloxazine ring (*43, 44*). The inconsistency of results between experimental and calculated FAD-dimer distances leaves the electron transfer mechanism between the catalytic cofactor and substrate undefined.

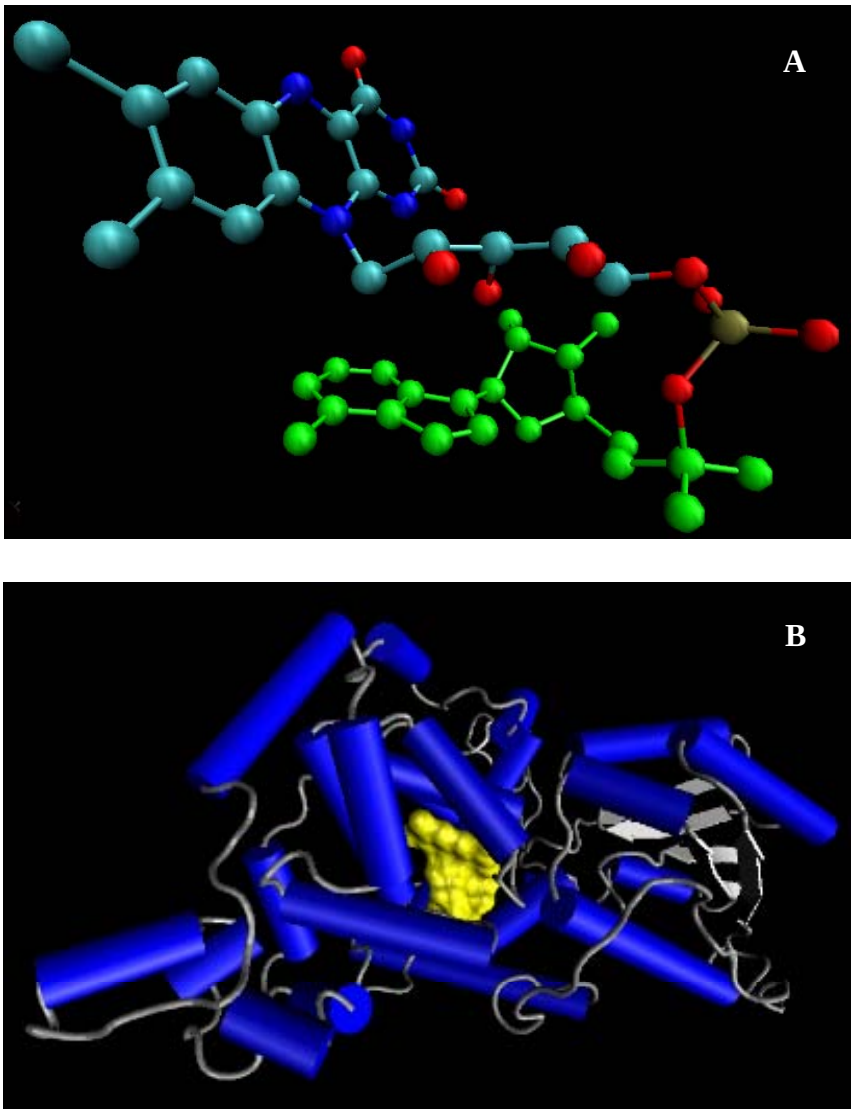

Figure 1.5. The Crystal Structure of *E. coli* Photolyase at 2.3 Å Resolution (*35*). (A) The FAD cofactor taken from the crystal structure of the holoenzyme, demonstrating the U-shaped conformation. Carbon atoms are shown in gray, nitrogen atoms in dark blue, oxygen atoms in red, phosphorus atoms in gold, and the adenine moiety is depicted in green. In (B) *E .coli* photolyase is shown with the bound flavin cofactor. The substrate binding site is at center where the flavin cofactor (in yellow) is exposed to the solvent. α-Helices are shown in blue, β-sheet structures are in white, and the peptide backbone is in gray. Structures were rendered using the program VMD (*45*) using the coordinate file *1DNP* obtained from the Protein Data Bank (*46*).

In summary, the biologically relevant DNA repair reaction has been studied extensively, but the final understanding of how the electron transfer proceeds from cofactor to substrate has not been confirmed. Pathways have been defined that require zero (*38, 39*), one (*40, 41*), or two [reviewed in (*47*)] intermediates for electron transfer, but the existence of any intermediate has yet to be demonstrated. Recent work has focused on the ability of amino acid sidechains to function in this regard, facilitating long distance electron transfer.

1.4 Amino Acid Radicals

Amino acid radicals can facilitate long range electron transfer by serving as intermediaries between the donor acceptor molecules. The first protein-bound amino acid radical to be discovered was the tyrosinate radical, the essential organic electron donor in ribonucleotide reductase (*48*). Tyrosyl radicals are the most extensively studied due to their prominent role in metabolism, photosynthesis, and respiration [reviewed in (*49, 50*)], but other amino acid radicals in proteins have since been identified, generated from glycine, cysteine, and tryptophan (*51*). Tryptophan is unique among the radical forming amino acids in that it can form both neutral and cationic radical species depending on the pH of the local environment (*52*).

A series of amino acid radicals as "hopping" points in biological electron transfer has been demonstrated in a mutationally-altered form of ribonucleotide reductase (*53, 54*) and in DNA photolyase (*55, 56*). In these two enzymes tryptophan acts as an intermediary redox center (*53, 56*). In photolyase, formation of tryptophan radicals has been experimentally observed during the light-driven process of photoactivation. *A.*

nidulans photolyase has been shown to generate a tyrosyl and a tryptophanyl radical to facilitate the FAD reduction reaction (*55*). In *E. coli* photolyase, the electron transfer chain may consist of three tryptophan residues, whose position and identity has been defined (*35, 56*). This "Trp triad" catalyzes the light driven reduction of FADH• to $FADH^-$ by sequential oxidation of tryptophan residues 382, 359, and 306 (*56*). It has also been postulated that a tryptophan radical is involved in the repair of cyclobutane pyrimidine dimers (*40, 41*), but as yet there is no direct experimental evidence.

1.5 Vibrational Spectroscopy

There are two main vibrational techniques, Fourier Transform infrared spectroscopy (FT-IR) and Raman spectroscopy. FT-IR allows characterization of covalent bonds in molecules by measuring the absorption of infrared light. The selection rules for FT-IR mandate that the molecule must undergo a change in dipole moment. Raman spectroscopy requires that the molecules of interest absorb the monochromatic light used for excitation and there must be a change in polarizability of the molecule.

The two methods are considered complementary because of their different selection rules. An advantage of Raman spectroscopy is that only molecules excited by the monochromatic light applied to the system will yield spectra, but this may also be considered a drawback, if different parts of the system studied require different wavelengths of light or components of the system fluoresce under the probe light. FT-IR does not suffer from this limitation and thus allows the simultaneous detection of all vibrational modes of the system. Because the technique is sensitive to individual bond

changes and bond energies, it is well suited to the detection of DNA damage and amino acid radical formation.

Vibrational studies of DNA have been limited mostly to measuring conformations adopted by the molecule. It has been demonstrated that contributions from base composition and tertiary structure [reviewed in (*57*)] are easily detected. Because samples can be studied in solution, base pairing and conformational transitions can be monitored as a function of solution state [reviewed in (*58*)]. More recent studies use vibrational spectroscopy to detect chemical changes in DNA from exogenous insult or as part of an enzymatic reaction (*59-61*). Chapter 2 of this thesis is an extension of these concepts, using FT-IR to probe a specific DNA lesion and understand the chemistry that is taking place in an oligonucleotide molecule.

Vibrational spectroscopy has also been used in the study of dynamic changes of redox active amino acids in proteins. Tyrosyl radicals have been characterized extensively by vibrational methods *in vitro* and *in vivo* [reviewed in (*51*)]. FT-IR is sensitive to changes in the redox state of amino acid sidechains, as well as to small changes in the amino groups involved (*62*). Vibrational spectroscopy of tryptophanyl radicals is currently in its infancy. The spectrum of ground state tryptophan has been presented in the literature, but not fully annotated (*63*). The FT-IR spectrum of the tryptophan sidechain analogue, 3-methylindole, has been obtained experimentally and assignment of vibrational modes based on theoretical calculations has been reported along with the calculated modes for the radical forms of the molecule (*64*). Chapter 3 of this thesis provides *in vitro* data on tryptophan modes in the ground state and *in situ*

observations of tryptophanyl radical formation in the electron transfer process of photorepair.

REFERENCES

1. Kelner, A. (1949) *Proc Nat Acad Sci U S A 35*, 629-638.
2. Sancar, G. B. (2000) *Mutat Res 451*, 25-37.
3. Minato, S., and Werbin, H. (1971) *Biochemistry 10*, 4503-4508.
4. Dulbecco, R. (1950) *J Bacteriol 59*, 329-347.
5. Ward, H. M. (1892) *Proc Roy Soc Lond 52*, 393-400.
6. Hollaender, A., and Claus, W. (1936) *J Gen Physiol 19*, 753-765.
7. Kelner, A. (1951) *J Gen Physiol 34*, 835-852.
8. Hershey, A. D., and Chase, M. (1952) *J Gen Physiol 36*, 39-56.
9. Watson, J. D., and Crick, F. H. (1953) *Nature 171*, 737-738.
10. Watson, J. D., and Crick, F. H. (1953) *Nature 171*, 964-967.
11. Beukers, R., Ylstra, J., and Berends, W. (1958) *Rec Trav Chim Pay B 77*, 729-732.
12. Sambrook, J., and Russell, D. W. (2001) pp A2.1, Cold Spring Harbor Laboratory Press, Cold Spring Harbor, New York.
13. Beukers, R., and Berends, W. (1960) *Biochim Biophys Acta 41*, 550-551.
14. Weinblum, D., and Johns, H. E. (1966) *Biochim Biophys Acta 114*, 450-459.
15. Varghese, A. J., and Wang, S. Y. (1967) *Nature 213*, 909-910.
16. Camerman, N., and Camerman, A. (1968) *Science 160*, 1451-1452.
17. Patrick, M. H., and Rahn, R. O. (1976) in *Photochemistry and Photobiology of Nucleic Acids* (Wang, S. Y., Ed.) pp 35-95, Academic Press, New York.
18. Douki, T., Court, M., and Cadet, J. (2000) *J Photochem Photobiol B 54*, 145-154.

19. You, Y. H., Lee, D. H., Yoon, J. H., Nakajima, S., Yasui, A., and Pfeifer, G. P. (2001) *J Biol Chem 276*, 44688-44694.

20. Rupert, C. S. (1960) *J Gen Physiol 43*, 573-595.

21. Li, Y. F., Kim, S. T., and Sancar, A. (1993) *Proc Natl Acad Sci U S A 90*, 4389-4393.

22. Sancar, A., and Sancar, G. B. (1984) *J Mol Biol 172*, 223-227.

23. Gindt, Y. M., Vollenbroek, E., Westphal, K., Sackett, H., Sancar, A., and Babcock, G. T. (1999) *Biochemistry 38*, 3857-3866.

24. Sancar, G. B. (1990) *Mutat Res 236*, 147-160.

25. Kim, S. T., and Sancar, A. (1991) *Biochemistry 30*, 8623-8630.

26. Heelis, P. F., and Sancar, A. (1986) *Biochemistry 25*, 8163-8166.

27. Heelis, P. F., Kim, S.-T., Okamura, T., and Sancar, A. (1993) *J Photochem Photobiol B 17*, 219-228.

28. Scannell, M. P., Fenick, D. J., Yeh, S.-R., and Falvey, D. E. (1997) *J Am Chem Soc 119*, 1971-1977.

29. Jorns, M. S., Wang, B. Y., Jordan, S. P., and Chanderkar, L. P. (1990) *Biochemistry 29*, 552-561.

30. Kim, S. T., Heelis, P. F., Okamura, T., Hirata, Y., Mataga, N., and Sancar, A. (1991) *Biochemistry 30*, 11262-11270.

31. Okamura, T., Sancar, A., Heelis, P. F., Begley, T. P., Hirata, Y., and Mataga, N. (1991) *J Am Chem Soc 113*, 3143-3145.

32. Payne, G., and Sancar, A. (1990) *Biochemistry 29*, 7715-7727.

33. Winkler, J. R., and Gray, H. B. (1997) *J Biol Inorg Chem 2*, 399-407.

34. Williams, R. J. P. (1997) *J Biol Inorg Chem 2*, 373-377.

35. Park, H. W., Kim, S. T., Sancar, A., and Deisenhofer, J. (1995) *Science 268*, 1866-1872.

36. Tamada, T., Kitadokoro, K., Higuchi, Y., Inaka, K., Yasui, A., de Ruiter, P. E., Eker, A. P., and Miki, K. (1997) *Nat Struct Biol 4*, 887-891.

37. Komori, H., Masui, R., Kuramitsu, S., Yokoyama, S., Shibata, T., Inoue, Y., and Miki, K. (2001) *Proc Natl Acad Sci U S A 98*, 13560-13565.

38. Antony, J., Medvedev, D. M., and Stuchebrukhov, A. A. (2000) *J Am Chem Soc 122*, 1057-1065.

39. Medvedev, D., and Stuchebrukhov, A. A. (2001) *J Theor Biol 210*, 237-248.

40. Hahn, J., Michel-Beyerle, M.-E., and Roesch, N. (1999) *J Phys Chem B 103*, 2001-2007.

41. Sanders, D. B., and Wiest, O. (1999) *J Am Chem Soc 121*, 5127-5134.

42. Mees, A., Klar, T., Gnau, P., Hennecke, U., Eker, A. P., Carell, T., and Essen, L. O. (2004) *Science 306*, 1789-1793.

43. Torizawa, T., Ueda, T., Kuramitsu, S., Hitomi, K., Todo, T., Iwai, S., Morikawa, K., and Shimada, I. (2004) *J Biol Chem 279*, 32950-32956.

44. Ueda, T., Kato, A., Ogawa, Y., Torizawa, T., Kuramitsu, S., Iwai, S., Terasawa, H., and Shimada, I. (2004) *J Biol Chem 279*, 52574-52579.

45. Humphrey, W., Dalke, A., and Schulten, K. (1996) *J Molec Graphics 14*, 33-38.

46. Berman, H. M., Westbrook, J., Feng, Z., Gilliland, G., Bhat, T. N., Weissig, H., Shindyalov, I. N., and Bourne, P. E. (2000) *Nuc Acids Res 28*, 235-242.

47. Weber, S. (2004) *BBA-Bioenergetics In Press*, doi:10.1016/j.bbabio.2004.02.010.

48. Sjoberg, B. M., and Reichard, P. (1977) *J Biol Chem 252*, 536-541.

49. Himo, F., and Siegbahn, P. E. M. (2003) *Chem Rev 103*, 2421-2456.

50. Stubbe, J. (2003) *Chem Commun*, 2511-2513.

51. Stubbe, J., and van Der Donk, W. A. (1998) *Chem Rev 98*, 705-762.

52. Jovanovic, S., Steenken, S., and Simic, M. (1991) *J Phys Chem 95*, 684-687.

53. Bleifuss, G., Kolberg, M., Potsch, S., Hofbauer, W., Bittl, R., Lubitz, W., Graslund, A., Lassmann, G., and Lendzian, F. (2001) *Biochemistry 40*, 15362-15368.

54. Sahlin, M., Lassmann, G., Potsch, S., Sjoberg, B. M., and Graslund, A. (1995) *J Biol Chem 270*, 12361-12372.

55. Aubert, C., Mathis, P., Eker, A. P., and Brettel, K. (1999) *Proc Natl Acad Sci U S A 96*, 5423-5427.

56. Aubert, C., Vos, M. H., Mathis, P., Eker, A. P., and Brettel, K. (2000) *Nature 405*, 586-590.

57. Tsuboi, M. (1969) *Appl Spectrosc Rev 3*, 45-90.

58. Liquier, J., and Taillandier, E. (1996) in *Infrared Spectroscopy of Biomolecules* (Mantsch, H. H., and Chapman, D., Eds.) pp 131-158, Wiley-Liss, New York.

59. Malins, D. C., Polissar, N. L., and Gunselman, S. J. (1997) *Proc Nat Acad Sci U S A 94*, 3611-3615.

60. Dovbeshko, G. I., Gridina, N. Y., Kruglova, E. B., and Pashchuk, O. P. (2000) *Talanta 53*, 233-246.

61. Schmitz, M., Tavan, P., and Nonella, M. (2001) *Chem Phys Lett 349*, 342-348.

62. Ayala, I., Range, K., York, D., and Barry, B. A. (2002) *J Am Chem Soc 124*, 5496-5505.

63. Mohan, S., Puviarasan, N., and Bakkialakshmi, S. (1999) *Asian J Chem 11*, 1137-1143.

64. Bunte, S., Jensen, G., McNesby, K., Goodin, D., Chabalowski, C., Nieminen, R., Suhai, S., and Jalkanen, K. (2001) *Chem Phys 265*, 13-25.

CHAPTER II

Vibrational Characterization of *In Vitro* Cyclopyrimidine Dimer Lesion in Nucleic Acids

ABSTRACT

Ultraviolet light induces DNA damage via formation of a covalent bond between adjacent pyrimidines, generating *cis-syn* cyclobutane pyrimidine dimers (CPD) as the most abundant primary lesion. Eight-base oligonucleotides, containing a central di-uracil, di-thymidine, or cyclobutane thymidine dimer flanked by purine bases, were measured using infrared methods, a critical step in probing DNA structure and charge distribution. Vibrational spectra of the model compounds thymine and thymidine served as references for pyrimidine modes in the oligonucleotides. Construction of a difference infrared spectrum of undamaged-minus-damaged DNA permitted the examination of changes in the nucleic acid upon formation of the cyclobutane dimer lesion between adjacent pyrimidines. Vibrational mode assignments were made based on comparison of *in vitro* spectra and mode frequencies and intensities from density-functional BLYP calculations with a 6-31G(d) basis set. Specifically, we noted alterations in the carbonyl and C-H modes between damaged and undamaged oligomers. In the carbonyl region of our difference data, we observe a negative infrared line at 1719 cm^{-1}, unique to the CPD lesion, and a broad, positive mode with intensity at 1757 and 1742 cm^{-1}, assignable to carbonyl groups in the di-thymidine containing oligonucleotide. The presence of the CPD lesion not only shifts methyl modes at 2941 and 2917 cm^{-1}, but also begets a novel 2961 cm^{-1} mode in the oligomer spectra. Preliminary assignments for these modes are the methyl groups attached to the C5 carbon and the C6-H stretch of thymidine ring, respectively. This vibrational study using oligonucleotides supports the application of this technique toward understanding the reactant and product of the repair of CPD lesions *in vitro*.

INTRODUCTION

There are many environmental agents that threaten the integrity of the genome through chemical modification of nucleic acid bases. Of these mutagens, one of the most potent is ultraviolet (UV) light. UV exposure has made skin cancer the most prevalent form of cancer in humans (*1*). Although the guanine and adenine molecules have a higher molar absorptivity (*2*), the initial insult by direct irradiation with short wavelength UV light is often dimerization of adjacent pyrimidine bases (*3*). Two possible UV-photoproducts from pyrimidine bases are the *cis-syn* cyclobutylpyrimidine dimer (CPD or T<>T for adjacent thymidine bases; Figure 2.1A) and 6-4 photodimers (*4*). Possibly resulting from the differing kinetics of photoproduct formation (*5*), the CPD lesion accounts for greater than 80% of all DNA photolesions (*6*).

Construction of the CPD lesion involves creation of two single bonds between thymine monomers by reduction of the C5=C6 double bonds in the two individual molecules. Theoretically, a number of steric outcomes are expected, as a result of bridging the thymine rings together. These include the likelihood that loss of the double bond between C5 and C6 may permit conformational flexibility in the pyrimidine ring. In contrast, formation of the CPD ring may also increase the strain within a number of bonds in the pyrimidine moieties and reduce the allowed positions for the C5 methyl and C6-H groups due to steric hindrance. Lastly, the CPD lesion may induce ring and bond strain in the ribose moiety or bond strain in the phosphodiester backbone.

Upon determination of methods to generate the cyclobutane pyrimidine lesion *in vitro* from DNA oligomers (*7-10*), research efforts focused on the elucidation of

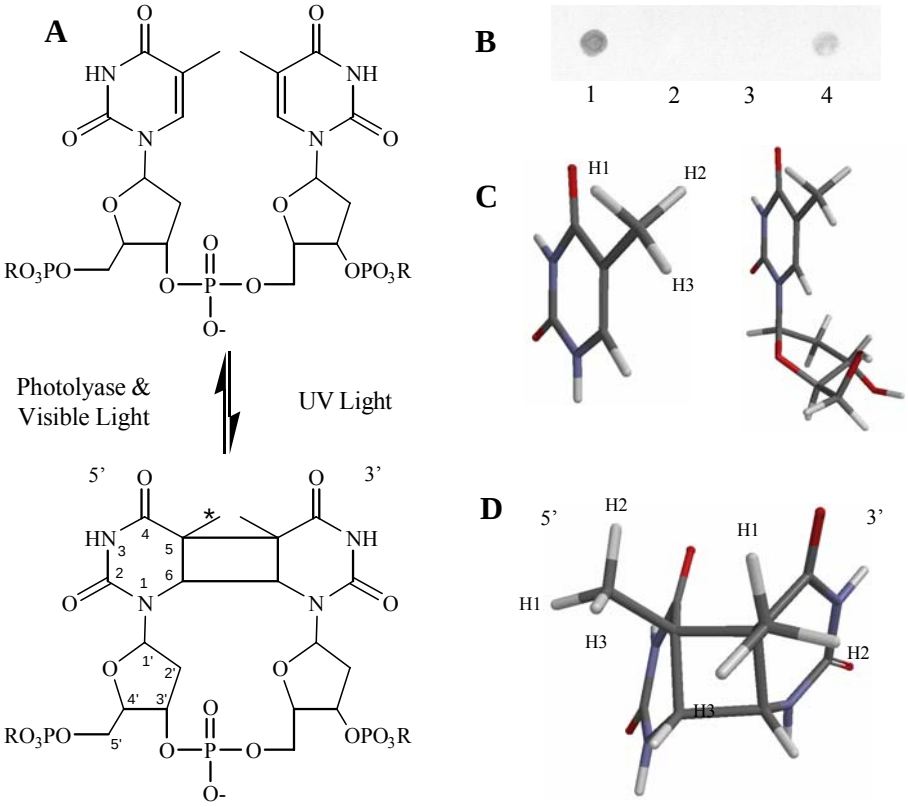

Figure 2.1. Chemical structure and detection of DNA containing CPD lesions. (A) DNA will form cyclobutane pyrimidine dimers in the presence of UV light. This damage can be catalytically reversed by the enzyme photolyase. The numbering system used throughout this work is presented in the lower panel of (A). In 8merUU, there is a hydrogen atom attached to the C5 position, whereas in 8merTT and 8merTTCPD the hydrogen is replaced by a methyl group. (B) Presence of a CPD lesion was detected using antibodies specific for the lesion. UV-irradiated plasmid DNA (1) and oligomer DNA (4) were detected using a chromogenic method. CPD lesions are absent in non-irradiated samples of plasmid (2) or oligomer (3). (C) Energy-minimized structures of the model compounds thymine and thymidine. Methyl hydrogen atoms are labeled in thymine, and are the same in thymidine. (D) Energy-minimized model of di-thymine CPD with positions for the methyl group hydrogen atoms labeled for both pyrimidine rings, based on their pre-dimerization positions. The designation of the 5' and 3' ends follows the convention used for DNA, and is applied to this structure as if it were in an oligonucleotide. The models presented in (C) and (D) were used to calculate vibrational modes and electrostatic potentials.

not only of its chemical composition but its structure, as the conformation of this molecule can affect the manner in which DNA repair proteins, such as photolyase, recognize and repair CPDs (Figure 2.1A) with exquisite specificity and efficiency (*11*). These efforts employed electron microscopy (*12, 13*), crystallography (*14-16*), magnetic resonance (*17, 18*), and computational (*19, 20*) methods. In addition to the structural change hypothesized in pyrimidine dimers, it has been postulated that the binding affinities of repair enzymes for CPD-containing DNA depend on the degree of unwinding or kinking caused by these chemical anomalies (*14, 21*). It is notable that, given the plethora of structural information obtained over the last three decades, there has been no consensus regarding the effect of CPD formation on duplex DNA. For example, there are discrepancies in the bond length and angles for dinucleotide dimers as determined by X-ray diffraction and NMR (*14, 17, 18*) and in the amount of DNA bending measured in the presence of CPDs (*13, 14, 17*).

Given the discrepancies between the studies above, one possible interpretation is that the cyclobutane pyrimidine lesion is conformationally flexible and susceptible to environmental conditions. Therefore, it is important to understand both the structure of pyrimidine dimers and its potential conformers during CPD formation and during its repair. In principle, vibrational spectroscopy can provide information about bond orders, charge distribution, and hydrogen bonding of individual groups. Using this biophysical technique, we can probe the structure of the thymine dimer under solution-state conditions, rather than under specific conformations stabilized by crystals. Most importantly, employment of these methods can elucidate not only the changes in the

molecules due to bond formation, but also the effect that dimerization has on the atoms not directly involved in the cyclobutane ring.

In this study, the vibrational spectra of three 8-base oligonucleotide derivatives have been obtained. The oligonucleotide (8merTT) is analogous to naturally occurring DNA. To elucidate changes that take place upon CPD lesion formation, a purified oligonucleotide containing a pyrimidine dimer (8merTTCPD) was generated. We report herein the first detailed description of the *in vitro* vibrational spectra of 8-base oligonucleotides in both non-damaged and CPD-containing forms. Vibrational spectra, obtained from thymine and thymidine, served as controls. As the presence and frequency of vibrational lines will be dependent on the presence of the ribose and phosphate moieties of oligonucleotides, mode assignments generated for model compounds are extended to more complex oligonucleotides. On the basis of density functional calculations, vibrational assignments are proposed. Dissection of these vibrational modes can be developed toward *in vitro* studies of thymine dimer repair mechanisms and toward the enzymatic mechanism by photolyase during photorepair.

EXPERIMENTAL PROCEDURES

Model compounds and DNA oligomers. Thymine and thymidine were obtained from Sigma (St. Louis, MO). Purchased from Sigma-Genosys (The Woodlands, TX), DNA oligonucleotides with the sequence GAATTAAG (8merTT) and GAAUUAAG (8merUU) were variable in purity. The oligomers were dissolved in sterile H_2O to ~150 μM and sterile-filtered using 0.45 μm Acrodisc syringe filters (Pall Gelman Laboratory, Ann Arbor, MI). The oligonucleotides were then HPLC purified (*14*) using a

Phenomenex (Torrance, CA) Luna 5µm RP-C18 column on a Shimadzu SL10A HPLC system. Starting with buffer E (100 mM triethylammonium acetate pH 7.0), the oligonucleotides were eluted with buffer F (100 mM triethylammonium acetate pH 7.0, 30% acetonitrile) using a two step gradient: 80 mL 0–20% buffer F, followed by 240 mL 20–50% buffer F. The purified oligomer eluted with 31% buffer F. The sample was lyophilized, and resuspended in sterile water to a concentration of 600 µM. The concentration of the purified DNA was determined by UV-vis spectroscopy, using extinction coefficients of 103,600 $M^{-1}cm^{-1}$ for 8merTT and 105,000 $M^{-1}cm^{-1}$ for 8merUU (*2*) at 260 nm.

To generate CPD lesion in the oligonucleotides (*8, 9*), 1.5 mL of oligomer DNA at a concentration of 195 µM in 75 mM potassium phosphate buffer pH 6.8 was degassed with nitrogen in stoppered quartz cuvettes (Starna, Atascadero, CA). Acetone (50 µL) and acetophenone (final concentration 5 mM) were added through a septum. The mixture was then irradiated with UV-B light (312 nm peak output, Spectronics, Westbury, NY) through a polystyrene Petri dish at 4ºC for 3 hours. The resulting 8merTT/8merTTCPD mixture was then lyophilized to remove acetone and acetophenone, and the damaged and non damaged DNA were separated using HPLC as above. Estimated from peak area in the HPLC chromatogram, the yield of dimerized products formed from this method is approximately 33% before purification. The concentration of 8merTTCPD was determined by UV-vis spectroscopy using an extinction coefficient of 90,000 M^{-1} cm^{-1} at 260 nm (*2, 22*).

Assays. An immunoblot assay (*6, 23*) was utilized to have positive proof of CPD formation in our DNA templates. In this procedure, 3.3 µg pAlter vector (Promega,

Madison, WI) and 6 µg 8merTT, in both UV-exposed and untreated forms, were applied to a polyvinylidene fluoride (PVDF) membrane (Millipore, Billerica, MA), presoaked in Tris-acetate EDTA pH 8.3 (TAE), with a BRL Hybri·Dot manifold (Life Technologies, Rockville, MD). Once dried to fix the samples to the membrane, the samples were equilibrated in wash buffer (10mM Tris pH 7.5, 150 mM NaCl), and then incubated for 1 hour in blocking solution (wash buffer with 3 g/L bovine serum albumin). As in standard immunoblotting procedures (*24*), a 1:1,000 dilution of the primary anti-CPD antibody TDM-2 [a generous gift from Prof. Tsukasa Matsunaga (Kanazawa Univ., Kanazawa Japan) (*23*)] and a 1:5,000 dilution of the secondary goat anti-mouse IgG horseradish peroxidase conjugate (Jackson ImmunoResearch, West Grove, PA) were incubated with the membrane in succession. The blot was then developed using a chromogenic method with 4-chloro-1-napthol as a substrate (*25*).

Vibrational spectroscopy. Note that all vibrational data shown herein are averages of at least three experiments, and were analyzed using IGOR Pro (Wavemetrics, Lake Oswego, OR). Infrared experiments were performed using a MCT/A detector in a Bruker IFS 66v/s infrared spectrometer under vacuum and at room temperature. Spectral conditions were: double-sided, forward-backward acquisition mode, Happ-Genzel apodization function, 20 kHz mirror velocity, 200 scans per interferogram, 1 level of zero filling, and gain of 1.

IR spectra of model compounds. In order to make tentative assignments on the IR spectra of damaged and non-damaged DNA, the IR spectra of the model compounds were obtained. Thymine and thymidine (>99% purity) were obtained from Sigma (St. Louis, MO) and used without further purification. Samples were mulled with potassium

bromide (approximately 1 mg sample per 80 mg KBr) using an agate mortar and pestle. The sample crystal was formed in a 7 mm die set with pressure applied using a hand press (Buck Scientific, Norwalk, CT) until a transparent pellet was formed. For FTIR spectroscopy, 200 scans at 2 cm^{-1} resolution were collected for each interferogram, which was 158 s in duration.

IR spectra of DNA substrates. To generate IR spectra of the cyclobutane lesion, oligomer DNA in both untreated and CPD-containing forms were purified as above. Twenty microliters of the 600 μM DNA solution was spotted on a CaF_2 window and dried under a stream of nitrogen (*26*). Once a solid residue was formed, the window was placed in a demountable cell (Harrick, Ossining, NY). Spectra were recorded at 2 cm^{-1} resolution.

Computational Methods. The Spartan '04 (Wavefunction Inc., Irvine, CA) software suite was used for all calculations. Vibrational modes, molecular orbitals, and electrostatic potentials were calculated from the equilibrium geometry using density functional theory (DFT) with the BLYP functional and a 6-31G* basis set. Although the software allows calculations using higher level functionals and basis sets, vibrational modes of model compounds calculated using the BLYP/6-31G* system agree well with experimental data (*20*).

RESULTS

Vibrational spectra of model compounds: thymine and thymidine. For reference, we have obtained experimental IR spectra of thymine and thymidine, as well as computationally determined the normal mode frequencies of these compounds (Tables 2.1 and 2.2). Thymine, one of the pyrimidine bases in genetic material, is a major

reactant in the biological photoreactions of DNA. As a consequence, there is a vast body of vibrational literature on thymine, and to a lesser extent thymidine, which are grounded in both theoretical and experimental techniques (*20, 27-35*). The twofold purpose of the control measurements was to: 1) establish that our methods and data acquired herein were in agreement with the literature and 2) map modes that may change upon lesion formation.

In this work, the model compound spectra were obtained in solid phase, in which there can be interactions between the model compound molecules in the mull. Experimental frequencies, obtained in our hands, and detailed mode assignments for these two compounds are compiled in Tables 2.1 and 2.2 for the 1800-1100 cm^{-1} low frequency and 3400-2800 cm^{-1} high frequency regions of the infrared spectrum, respectively. These data are in good agreement with previous reports of polycrystalline thymine and thymidine (*27-30, 32-43*). Assignment of our experimental data was bolstered by *ab initio* calculations of vibrational modes of thymine and thymidine, and supported by DFT calculations on electronic structure. Vibrational modes calculated for the model compounds correspond well to values reported in the literature (*20, 27-29, 32, 34, 35, 37, 41, 42, 44, 45*), and are consistent with measured values.

For planar thymine, we expected a maximum of 39 fundamental modes, as the total number of vibrational modes is 3N-6 for a nonlinear compound containing N-atoms. Group frequency and experimental data support broad, generalized assignment of vibrational frequencies to different functional groups. Only the fundamental stretching modes of O-H, N-H, and C-H groups are localized in the 3600-2800 cm^{-1} region. In contrast, the 1800-1000 cm^{-1} spectral window contains a complex amalgam of modes,

Table 2.1. Low Frequency Vibrational Mode Assignments for Thymine and Thymidine. Averages of three independent spectra of thymine and thymidine in KBr pellets were obtained; the frequency of infrared lines from the experimentally (expt) determined spectra are presented. The vibrational frequencies of thymine and thymidine were calculated using DFT-BLYP/6-31G*, and are the unscaled values (calc). Abbreviations: ν, stretching; δ, bending; δ_a, asymmetric bending; δ_s, symmetric bending; r, rocking; sc, scissoring; w, wagging; (-), not applicable; and (nd), not determined.

Tentative Mode Assignments[a]	Thymine		Thymidine		Tentative Assignment of Thymidine Specific Modes[b]
	Expt	Calc	Expt	Calc	
ν(C2=O)	1736	1763	1709	1717	
ν(C4=O)	1677	1705	1699	1704	
ν(C5=C6)	1677	1646	1659	1631	
ν(Ring)	1481	nd	1478	nd	
	-	-	1457	1462	sc(C5'-H_2)
δ(N1-H)	1446	1444	-	-	
$\delta_a(CH_3)$	1427	1487	1435	1489	
	-	-	1412	nd	sc(C2'-H_2)
	-	-	1401	1398	r(C5'-H_2), ν(Ring)
δ(N3-H)	1405	1353	1391	1338	
$\delta_a(CH_3)$	1383	1465	1383	1466	
δ(C6-H)	1366	1370	1383	1380	
$\delta_s(CH_3)$	1366	1409	1363	1419	
	-	-	1352	1353	δ(C4'-H)
	-	-	1335	1338	δ(C1'-H), ν(Ring)
	-	-	1290	1289	δ(C'-H), ν(Ring), ν(Ring')
ν(Ring)	1256	nd	nd	nd	
ν(Ring)	1245	nd	nd	nd	
	-	-	1224	1228	δ(C'-H), ν(Ring)
ν(C5-CH_3)	1215	1188	1253	1218	
	-	-	1197	nd	ν(Ring)
	-	-	1172	1168	δ(C'-H), δ(O'-H), ν (Ring)
	-	-	1121	1125	w(C2'-H), δ(C'-H)

[a] Tentative vibrational mode assignments for modes common to both thymine and thymidine were made from published assignments (*20, 27-35*) and our own calculated and experimental work.

[b] The vibrational modes specific to thymidine were tentatively assigned based on the available literature (*43, 44*) and our calculated and experimental data.

Table 2.2. High Frequency Vibrational Mode Assignments for Thymine and Thymidine. Averages of three independent spectra of thymine and thymidine in KBr pellets were obtained; the frequency of infrared lines from the experimentally (expt) determined spectra are presented. The vibrational frequencies of thymine and thymidine were calculated using DFT-BLYP/6-31G*, and are the unscaled values (calc). Abbreviations: ν, stretching; δ, bending; δ_a, asymmetric bending; δ_s, symmetric bending; r, rocking; sc, scissoring; w, wagging; (-), not applicable; and (nd), not determined.

Tentative Mode Assignments[a]	Thymine		Thymidine		Tentative Assignment of Thymidine Specific Modes[b]
	Expt	Calc	Expt	Calc	
	-	-	3311	3530	ν (O5'-H)
	-	-	3311	3520	ν (O3'-H)
ν(N1-H)	3194	3447	-	-	
ν(N3-H)	3175	3411	3156	3410	ν (N3-H)
ν(C6-H)	3062	3072	3086	3087	ν (C6-H)
	-	-	2994	3009	ν_a(C2'-H)
$\nu_a(CH_3)$	nd	2990	nd	2986	$\nu_a(CH_3)$
	-	-	2977	2981	ν (C1'-H)
$\nu_a(CH_3)$	2963	2962	2963	2954	$\nu_a(CH_3)$
	-	-	nd	2941	ν_s(C2'-H)
	-	-	nd	2923	ν (C3'-H)
$\nu_s(CH_3)$	2930	2914	2933	2908	$\nu_s(CH_3)$
	-	-	2898	2903	ν_a(C5'-H)
	-	-	nd	2872	ν (C4'-H)
	-	-	2836	2848	ν_s(C5'-H)

[a] Tentative vibrational mode assignments for modes common to both thymine and thymidine were made from published assignments (*20*, *27-35*) and our own calculated and experimental work.

[b] The vibrational modes specific to thymidine were tentatively assigned based on the available literature (*43*, *44*) and our calculated and experimental data.

such as (a) the carbonyl and C=C modes at 1760–1600 cm^{-1}, (b) C-C/C-N ring and N-H modes at 1600–1450 cm^{-1}, (c) methyl bending and ring vibrations at 1450–1360 cm^{-1}, (d) ribose ring vibrations at 1360–1250 cm^{-1}, and (e) ring, methyl bending, and C-H vibrations at 1250–1100 cm^{-1}.

The theoretical and experimental data reported herein (Tables 2.1 and 2.2) clearly show that thymidine demonstrates comparable modes to thymine. The addition of the ribose ring increases the number of vibrational normal modes to 87 (3N-6, where N=31). The addition of the ribose moiety not only increases the number of vibrational lines, but alters the normal mode description of the thymine base. For example, we have identified modes specific to the ribose ring in the 1350 to 1275 cm^{-1} region of the spectrum, which are not present in thymine spectra, and carbonyl modes in the 1800 – 1650 cm^{-1} region that may be useful for observing perturbation of the DNA molecule.

Isolation and vibrational characterization of CPD lesion in oligomers. Using single-stranded oligomers, we generated and purified an oligomer containing a centrally located CPD lesion, using published methods (*9, 46*). An octamer with a centrally located thymine pair [GAATTAAG, 8merTT] was selected to eliminate the possibility of end-to-end oligomer linkage between terminal thymines (*46*) and to minimize vibrational complexity and interpretation. As demonstrated by anti-CPD antibody reaction in an immunoblot (Figure 2.1B), damaged, or UV-irradiated, oligomers and plasmids in our hands contain CPD-type lesions, whereas negative control plasmid and oligomer DNA samples did not exhibit any reaction with the anti-CPD antibody. Therefore, we refer to the UV-irradiated oligomer as 8merTTCPD.

Previously, vibrational spectra of oligo- and poly-nucleotides have been analyzed with the objectives of assigning modes to the macromolecular structure that these biological molecules may adopt (*47-49*) and identifying marker modes for individual nucleic acid components (*38, 45, 50-53*). These studies cumulatively argue that, although the spectrum of a macromolecule is very complex, key structural features and contributions from individual nucleic acids can be determined. With this body of analysis in hand (*45, 47-49, 54, 55*), we demonstrate that variations in the frequency of modes between 1340-1200 cm^{-1} can be employed to discriminate aberrations in the chemical composition and macromolecular structure of specific nucleic acids *in vitro*.

In Figure 2.2, we present this aforementioned region of the infrared absorbance spectra, obtained from three different 8-base oligonucleotides, containing a pair of centrally localized thymidines (8merTT), a pair of deoxyuridines (8merUU), or a cyclobutyl thymidine dimer (8merTTCPD). The absorbance spectrum of 8merTT (Figure 2.2A, solid line) exhibits vibrational lines at 1331, 1292, 1277, and 1229 cm^{-1}. This 1340-1200 cm^{-1} region encompasses weak NH vibrations and CH in-plane deformations of nucleic acids above 1270 cm^{-1}, as well as strong, asymmetric stretching vibrations (ν_a) of PO_2^- at ~1235 cm^{-1}.

The majority of these modes provide markers for individual nucleic acid components, and are expected to be similar in intensity and frequency in the 8merUU and 8merTTCPD spectra. The 1292 cm^{-1} line has been assigned to a composite of pyrimidine ring, (C'-H) bending (δ), and ribose ring vibrations of thymidine based on isotope edited studies of thymidine (*43, 44*). Consistent with this interpretation, the 8merUU spectrum exhibits an identical infrared line at 1292 cm^{-1} (Figure 2.2B); note that there is a small

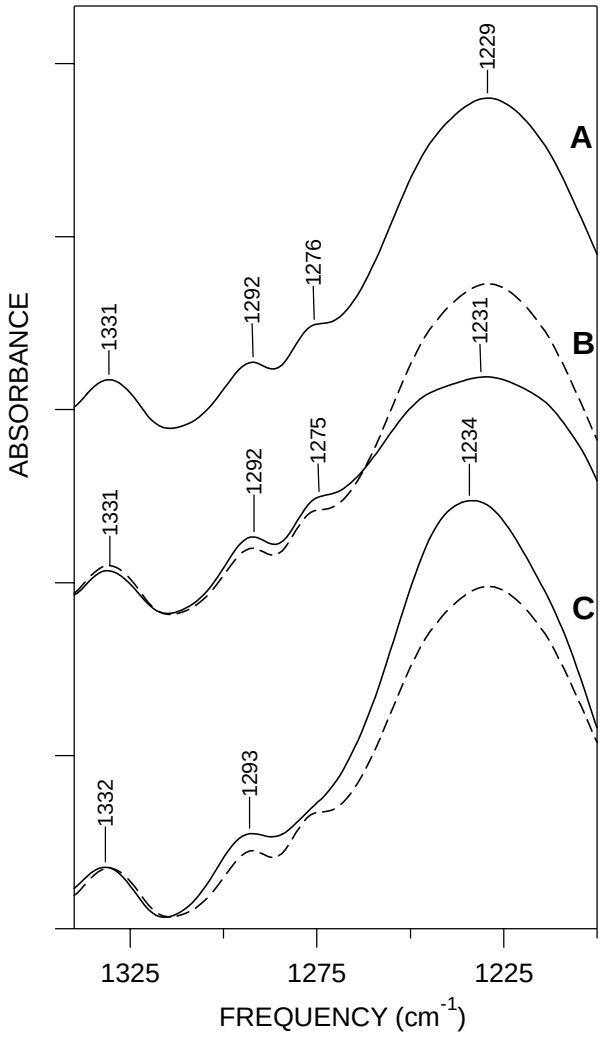

Figure 2.2. The 1340-1200 cm^{-1} region of infrared spectra of single-stranded oligonucleotides. The absorbance spectrum (A) is 8merTT. In (B) the absorbance spectrum of 8merUU (solid line) is shown. (C) the absorbance spectrum of 8merTTCPD (solid line). The 8merTT spectrum is shown for reference as a dashed line in B and C. The tick marks on the y-axis represent 0.03 absorbance units.

upshift in frequency to 1293 cm^{-1} in the 8merTTCPD spectrum (Figure 2.2C) presumably attributable to the chemical modification of the pyrimidine rings involved in CPD formation. In addition, the observed 1331 and 1276 cm^{-1} lines in 8merTT (Figure 2.2A) represent canonical markers of adenosine or thymidine in a DNA molecule (*49, 50, 54*). Although both of these infrared modes are nearly identical in the 8merUU and 8merTT data (Figure 2.2B), they shifted in frequency in the 8merTTCPD spectrum (Figure 2.2C). These data indicate that the 1331, 1292, and 1276 cm^{-1} lines provide information of the chemical composition of the oligonucleotides probed herein. In particular, the absence of the 1276 cm^{-1} mode may provide a unique gauge for monitoring the formation of CPD lesions in adjacent thymidines.

The infrared spectra of oligonucleotides also provided evidence that changes in the macromolecular structure of the DNA molecule take place upon formation of the CPD lesion. The strong infrared line at 1229 cm^{-1} in the 8merTT spectrum is tentatively assigned to $\nu_a(PO_2^-)$. Upon formation of the C-C bonds between the adjacent thymidines, the ν_a vibration(s) of the PO_2^- groups shift from 1229 cm^{-1} in 8merTT to 1234 cm^{-1} in 8merTTCPD (Figure 2.2C), and also change in line shape. Given that vibrations of phosphate groups are conformationally sensitive (*50*), these data show structural perturbations due to the presence of the CPD lesion in the single-stranded oligonucleotide. We conclude that, in solution, these 8-base oligomers can occupy a variety of conformational states, which differ in the geometry of the phosphate backbone.

Reciprocal vibrational modes in model compound and in single-stranded oligonucleotides. Our second and more important experimental goal was to map the changes in bond orders and charge distribution in thymidine that occur upon formation of

the CPD lesion. Toward this end, we compared experimental data derived from the model compounds, thymine and thymidine (Figure 2.1C), with data derived from computational methods. Computational chemistry offers ways to explore these lesions at the atomic level in controlled, known conditions nearly impossible to achieve experimentally. However, note that although computational efforts can facilitate the understanding of FT-IR spectra of compounds, there are limitations in the models chosen, due to size restraints of accessible, computational thresholds. The largest molecule we examine *in silico* is the di-thymine dimer (Figure 2.1D). Of foremost interest in this comparison are the alterations of frequencies from the reciprocal carbonyl, methyl, and C-H modes across all molecular entities examined, as large chemical perturbations are expected for these functional groups during CPD formation and repair (Figure 2.1).

Carbonyl stretches of model compounds and oligonucleotides. In thymine, there are carbonyl groups located at the C2 and C4 positions of the ring (Figure 2.1A). Carbonyl modes have high infrared extinction coefficients and are spectrally distinct due to their position in the infrared spectrum. Consequently, vibrational lines derived from these species are readily apparent in the 1790-1660 cm^{-1} region of the spectrum, and can be ascribed to in-plane stretching motions of the C=O species. The shift in frequency of C=O stretches reflect changes in double bond character in the C=O bond, as well as the environment of the molecule. For example, in the gas phase, or an inert matrix to simulate the gas phase, little interaction between thymine molecules occurs, generating few hydrogen bonded thymine pairs. Different levels of hydrogen bonding will shift carbonyl peaks observed at 1660 cm^{-1} in aqueous solution (*32*) to frequencies as high as 1775 cm^{-1} in Ar matrices (*30, 33, 34, 40*).

Comparison of thymine and thymidine yields prediction of the behavior of ν(C=O) and ν(C=C) vibrational modes upon addition of substituents to the thymine ring. In the polycrystalline state utilized in this work, thymine displays two intense vibrational lines at 1736 and 1677 cm^{-1} in the infrared spectrum (Figure 2.3A), which were attributed to the C2=O and degenerate C4=O/C=C modes (*27, 28, 30, 32-35, 41, 56*). In thymidine, the addition of a ribose group to the thymine ring structure results in loss of degeneracy, a vibrational shift, and the appearance of two distinct, infrared carbonyl modes at 1709 and 1699 cm^{-1} (Figure 2.3B). Furthermore the C=C stretching component of the 1677 cm^{-1} line, arising from the combined C4=O/C5=C6 mode in thymine (*27, 29, 32, 35, 36, 42*), downshifts to 1659 cm^{-1} in thymidine (Figure 2.3B)(*32, 37*). The calculated carbonyl modes agree with this interpretation of vibrational mode shifts (Table 2.1).

Taken together experimental and theoretical data indicate that substitutions to the thymine ring can trigger substantial perturbations of both the C=C and carbonyl modes, even when these atoms are not directly bonded to the changed ring substituent. This is applicable to the formation of CPDs, where the major change to the pyrimidine ring, besides loss of a double bond, can be seen as a substitution to two positions on the thymine ring. The addition of mass to the ring, along with perturbations to ring structure and potential, is expected to have marked effects on the vibrational spectrum.

In the 1825-1550 cm^{-1} region, the spectral complexity should increase for oligonucleotides, due to a larger number of functional groups in the molecule. There are five infrared lines at 1760, 1693, 1644, 1599, and 1573 cm^{-1} in the 8merTT spectra (Figure 2.3C). The presence of additional bases and phosphate linkages in the oligonucleotide modifies both the number and range of carbonyl and C=C modes. In the

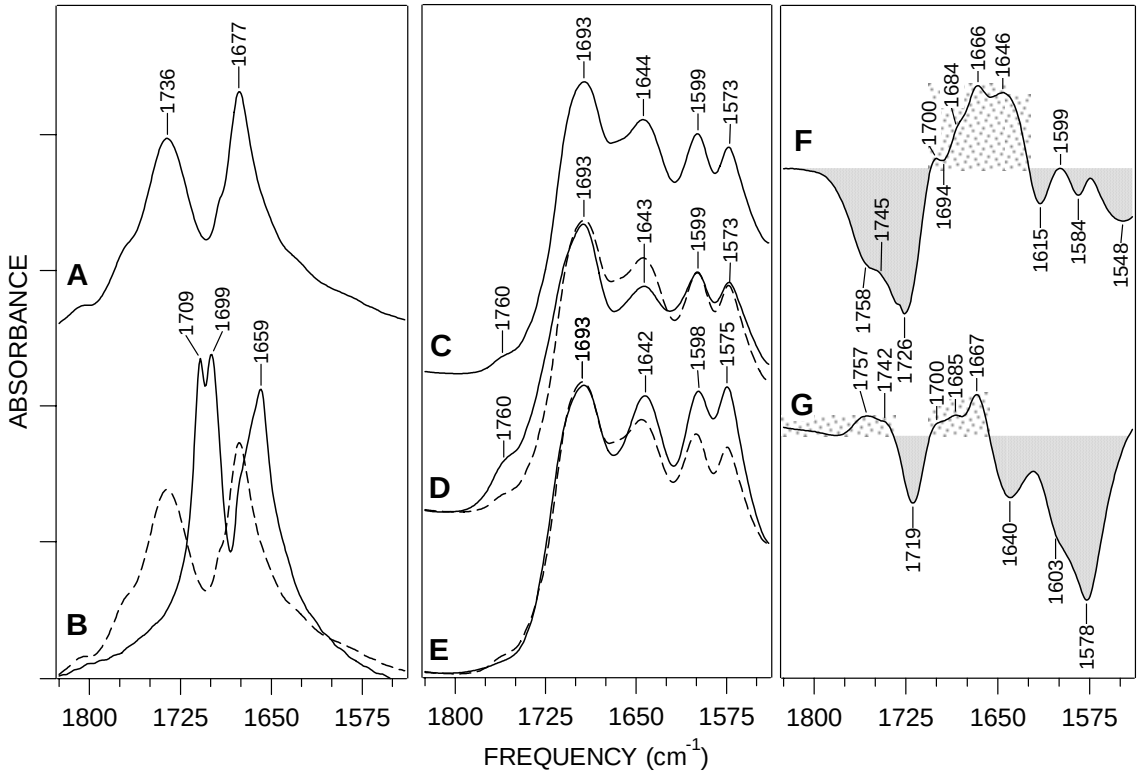

Figure 2.3. **The 1825-1550 cm^{-1} region of infrared spectra of the model compounds and oligonucleotides.** Shown are the double bond stretching modes of (A) thymine and (B) thymidine. To highlight vibrational shifts upon addition of ribose to thymine, the spectrum of thymine (B, dashed line) is superimposed on the spectrum of thymidine. Also shown are the absorbance spectra of (C) 8merTT, 8merUU (D, solid line), and 8merTTCPD (E, solid line). The spectrum of 8merTT is shown for reference as a dashed line in (D) and (E). The absorbance data in (C) – (E) were scaled based on intensity at 1693 cm^{-1}. (F) The 8merTT-minus-8merUU difference spectrum. (G) The 8merTT-minus-8merTTCPD difference spectrum. The absorbance scale is 0.33 absorbance units per tick, 0.04 absorbance units per tick in the first two panels, respectively. In the difference spectra the scale is Δ 0.015 absorbance units per tick.

8merUU spectrum, we expected to observe structural and/or electrostatic effects due to the removal of methyl groups on C5 of thymine. Alterations in the 8merUU infrared data (Figure 2.3D, solid line) included increased intensity of the 1760 cm^{-1} mode, change in line shape for the 1693 cm^{-1} line, and decreased amplitude of the 1643 cm^{-1} line.

To facilitate dissection of vibrational modes specific to the central pyrimidines in the oligonucleotides, we generated difference spectra of 8merTT-minus-8merUU (Figure 2.3F). Positive lines in this difference spectrum arise from the consequences of the methyl group on C5 of two thymines in the oligonucleotides, whereas negative lines are unique modes from the absence of the methyl groups. There are two negative lines at 1758 and 1726 cm^{-1} (Figure 2.3F), arising from 8merUU, and positive lines at 1700 and 1666 cm^{-1}, as well as a shoulder at 1684 cm^{-1}, arising from 8merTT. The positive modes at 1666 and 1646 cm^{-1} (Figure 2.3E) partially derive from the C=C bonds in the thymidine. The C=C bonds of 2-deoxyuridine are expected to be present at 1644 cm^{-1}, but the intensity of this mode is much lower in 2-deoxyuridine than in thymidine (*32, 57*).

Inspection of the 8merTTCPD absorbance spectrum (Figure 2.3E, solid line) highlights distinct changes in the carbonyl stretching region. The vibrational line at 1760 cm^{-1}, present in both 8merTT and 8merUU (Figure 2.3C and D), is not detectable in 8merTTCPD (Figure 2.3E, solid line), but vibrational lines at 1650-1570 cm^{-1} range were intensified. In the 8merTT-minus-8merTTCPD difference spectrum (Figure 2.3G), there was a broad, positive mode with notable intensities at 1757 and 1742 cm^{-1}, arising from unique mode(s) in non-damaged DNA, and a negative line at 1719 cm^{-1} (Figure 2.3F), which arises from unique structural changes in the 8merTTCPD oligonucleotide. Additional positive vibrational lines at 1700, 1685, and 1667 cm^{-1} (Figure 2.3F) arose

from carbonyl stretching modes, and the 1667 cm^{-1} line may have contributions from the carbonyl stretching modes and/or from the C5=C6 stretching mode.

C-H modes of model compounds and oligonucleotides. Measurement of the thymine C5-methyl group properties may provide structural information about the CPD lesion. For example, upon formation of the CPD lesion, there may be conformations of the methyl groups in thymidine that are no longer accessible. Thus, we next focus on the spectral regions, in which there may be contributions from C-H modes. The C-H stretching modes can be divided into two groups: harmonic stretching at the C6 position and the group stretching of the methyl hydrogen atoms. Associated with each type of C-H stretching mode are asymmetric and symmetric descriptors.

The experimental 3100-2700 cm^{-1} spectral window (Table 2.2) contains relatively isolated, fundamental stretching modes of a hydrogen atom attached to carbon in the pyrimidine ring common in both thymine and thymidine. In general, the C6-H stretching motions in the pyrimidine ring are the highest energy mode for both molecules in this region, and sugar C'-H stretching modes are downshifted between 90-250 cm^{-1} for thymidine. The vibrational line at 3062 cm^{-1} is representative of C6-H stretching of thymine. Addition of the ribose ring at the N1 positions causes an upshift of the ν(C6-H) vibrational line to 3086 cm^{-1}. We observe two experimental lines in both the thymine and thymidine data (Table 2.2) at 2963 cm^{-1} and ~2930 cm^{-1}, assigned to the asymmetric and symmetric stretching modes of the methyl group.

The experimental 3100-2700 cm^{-1} region (Table 2.2) also contains ν(C'-H) modes of the ribose moiety of thymidine. Vibrational lines for C'-H stretching in ribose have been reported for the C2' and C5' positions (*43, 44*). The vibrational line at 2977 cm^{-1}

was detected in our experimental data and is tentatively assigned to C1'-H stretching based on the calculated frequency of 2981 cm^{-1}. The 2836 cm^{-1} line in our experimental data is tentatively assigned to C5'-H stretching based on the calculated frequency of 2848 cm^{-1}. Although C-H stretches of C2', C3', and C4' in ribose have been calculated (Table 2.2) at 2981, 2941, and 2923 cm^{-1}, respectively, there are no apparent experimental counterparts. Shown in Figure 2.4 are the infrared spectra from the oligonucleotide 8merTT, 8merUU, and 8merTTCPD molecules in the C-H region. Akin to the 2977 cm^{-1} line detected in thymidine (Table 2.2), we observe a 2978 cm^{-1} mode in 8merTT (Figure 2.4A) and 8merTTCPD (Figure 2.4C, solid line) oligomer data. This line has been assigned as C-H stretching in the ribose ring (*32*), and we argue that it likely arises from the ribose ν(C1'-H). However, changes in pyrimidine composition yielded an alteration of the 2978 cm^{-1} line shape in both the 8merUU (Figure 2.4B, solid line) and 8merTTCPD (Figure 2.4C, solid line) spectra in comparison to 8merTT (Figure 2.4A). Moreover, this 2978 cm^{-1} line is shifted in frequency to 2974 cm^{-1} in the absence of the methyl groups at C5 in the 8merUU oligomer (Figure 2.4B, solid line). In the 8merTT-minus-8merUU difference spectrum (Figure 2.4C), we clearly observe that a positive 2990 cm^{-1} line is replaced by a negative 2971 cm^{-1} line, when uracil bases are exchanged for thymines in the oligomer. These observed frequencies for pyrimidines in nucleic acid strands are perturbed, compared to isolated pyrimidines. Taken together, we tentatively assign the positive 2990 cm^{-1} and negative 2971 cm^{-1} lines to the C1'-H the stretching modes of 2-deoxythymidine and 2-deoxyuridine in oligonucleotides, respectively (*57*).There are three candidate modes for the methyl group at C5 (Figure 2.1A) in the absorbance spectrum of the 8merTT oligomer: these modes should be absent in the

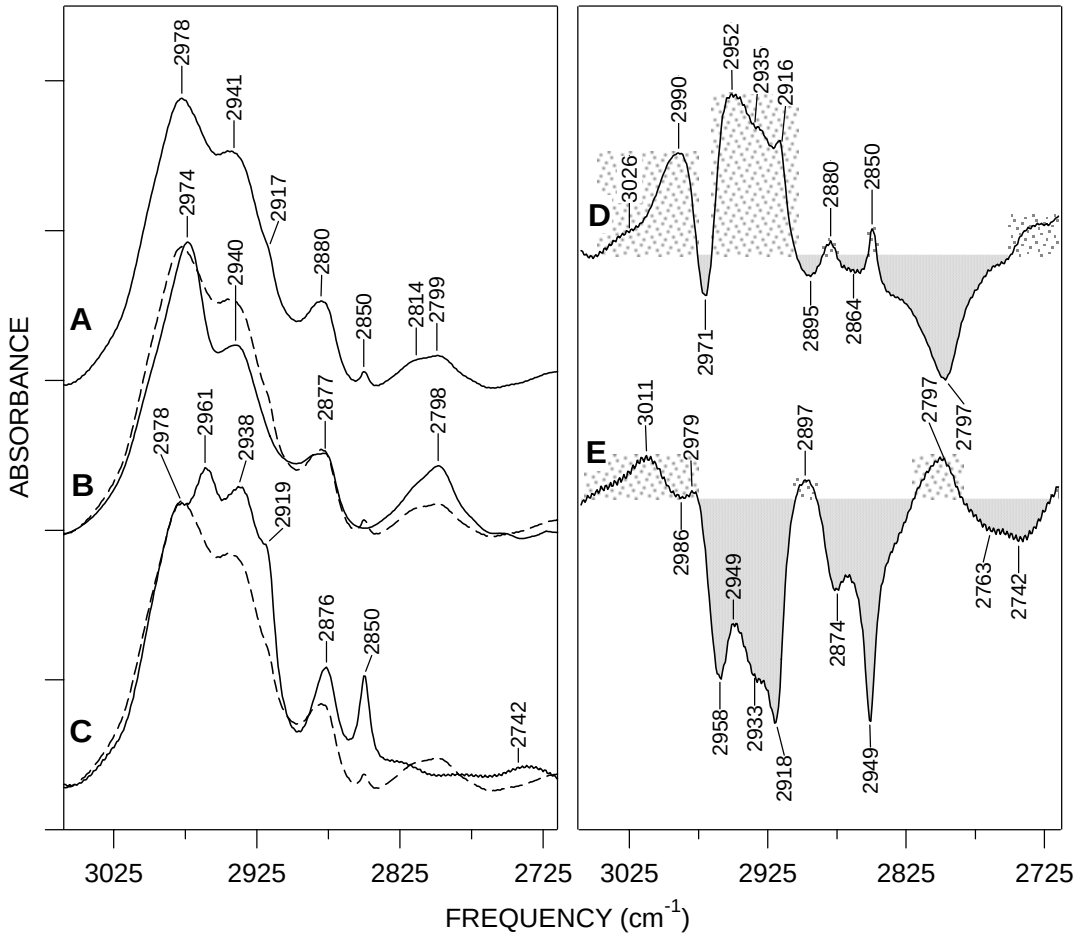

Figure 2.4. Fundamental C-H stretching modes. Shown are (A) the 8merTT absorbance spectrum, (B), the 8merUU absorbance spectrum (solid line), and (C) the 8merTTCPD absorbance spectrum (solid line). For reference the 8merTT absorbance spectra is repeated as a dashed line in (B) and (C). The absorbance spectra were scaled based on intensity at 2978 – 2974 cm^{-1}. Shown are the (D) 8merUU-minus-8merTT difference spectrum and (E) the 8merTT-minus-8merTTCPD difference spectrum. The y-axis tick marks for the absorbance spectrum represent 0.01 absorbance units, in the difference spectrum the tick marks represent Δ 3.4 x 10^{-3} absorbance units.

8merUU sample and may be altered in the 8merTTCPD data. For example, the 2850 cm^{-1} line from the 8merTT sample (Figure 2.4A) does not have a counterpart in the 8merUU data, but has increased amplitude in the 8merTTCPD spectrum (Figure 2.4C, solid line). We also note that a 2941 cm^{-1} mode and its associated shoulder at 2917 cm^{-1} in the 8merTT data (Figure 2.4A) have decreased amplitude in the 8merUU spectrum (Figure 2.4B). This difference is highlighted in Figure 2.4D, where a broad positive mode between 2952-2916 cm^{-1} and a sharp, positive 2850 cm^{-1} line are associated solely with the presence of a methyl group on C5 in the central pyrimidines. In the 8merTTCPD spectrum (Figure 2.4C), these modes are shifted in frequency to 2938 and 2919 cm^{-1}. Thus, we tentatively assign components of our observed, broad 2941/2917 cm^{-1} lines, as well as the 2850 cm^{-1} line, to the C-H stretching of the thymine methyl group.

The presence of the CPD lesion in oligomers also correlates with the appearance of unique vibrational modes in the 3000-2800 cm^{-1} region. The absorbance spectrum of 8merTTCPD (Figure 2.4C, solid line) has a singular vibrational line at 2961 cm^{-1}, and it is represented by the negative 2958 cm^{-1} feature in the 8merTT-minus-8merTTCPD difference spectrum (Figure 2.4E). Based on our model compound data on thymidine (Table 2.2), this singular infrared line may result from perturbation of a methyl mode or a C'-H stretch of the ribose functionality. A third hypothesis is that, upon alteration of the nature of the C6-H bond in the pyrimidine ring in the presence of a CPD lesion, the ν(C6-H) is downshifted from frequencies greater than 3000 cm^{-1}.

DISCUSSION

The interaction of nucleic acids with enzymes has been studied by vibrational methods. These biological interactions require that a nucleic acid adapt to a variety of physiological conditions, which in turn demands conformational flexibility between the base, ribose sugar, and phosphate moieties. The majority of vibrational studies have focused on using spectroscopy to measure structure and force fields of genetic material. In contrast, our long-range goal is to explore the chemical interplay of the bases in genomic lesions with enzymes responsible for DNA repair.

Toward this end, we report the generation and assignment of infrared spectra of the cyclobutane pyrimidine lesion localized within an oligonucleotide, a critical step in probing DNA structure and charge distribution with vibrational spectroscopy. Other groups have used FT-IR spectroscopy to separate the four possible dimers formed from irradiated thymine (*58*) or to assign the modes of the thymine dimer, but the focus was on the *trans-anti* dimer (*59*), which is not believed to occur *in vivo* (*16*). It is essential that DNA lesions be observed in their more appropriate biological context, i.e. as part of poly- or oligonucleotides. Use of a larger polymeric framework around the CPD lesion enables us to detect the extent of effects that lesion formation has on the macromolecule, and in the immediate vicinity of the lesion.

Oligonucleotides adopt conformations based on their sequence and local environment (*54*). Vibrations of the phosphate group are found to be conformationally sensitive. Raman and infrared lines have been measured and assigned to the A, B, and Z conformations of synthetic oligonucleotides and native DNA. Z-DNA, which is a left-handed helix, is dependent upon sequence and not readily adopted by oligonucleotides

that are A-T rich (*54*), such as the ones used in this study. A right-handed helix, B-DNA is the most common DNA conformation, and is the natural structure for DNA in solution. Dessication, or removal of water, shortens the double helix, compacting and forming the less extended A conformation of DNA.

Keeping in mind that resolution of whether ssDNA adopts regular helical conformations is under debate, we report an upshift of frequency for phosphate modes in the presence of a central CPD lesion. Resultant from the shorter distance between PO_2^- groups and distortion of the torsion angles in the phosphodiester backbone (*50*), the $\nu_a(PO_2^-)$ marker bands for A-DNA are upshifted 11 cm^{-1} relative to the B form. Thus, we conclude that the change of infrared frequency from 1231 cm^{-1} to 1234 cm^{-1} (Figure 2B and 2C) in our spectra clearly indicates a distortion of the phosphate backbone. This interpretation is consistent with both x-ray crystallographic and NMR solution studies of CPD lesions (*14, 17*). The detection of a shift in phosphate vibrational modes demonstrates the utility of FT-IR in detecting aberrant DNA conformations related to DNA damage.

Carbonyl stretches of CPD lesions in oligonucleotides. In order for DNA damage to have a direct effect on carbonyl stretching modes in an oligonucleotide, these functional groups must be part of the base involved in lesion formation. Whereas cytidine and guanidine each have one carbonyl group, thymidine is unique in that it has two such chemical groups. The presence of two carbonyls, which are prominent in IR spectra, provide a method for detection of DNA damage specifically at thymidine residues. The positive lines at 1757 and 1742 cm^{-1} in the 8merTT-minus-8merTTCPD

difference spectrum (Figure 2.3G) display an energy gap of 15 cm^{-1}, similar to the calculated energy gap between C2 and C4 in thymidine (Table 2.1).

We observed shifts in carbonyl stretching modes upon lesion formation that result in a distinct 1719 cm^{-1} vibrational line (Figure 2.3). To provide tentative assignment of this unique carbonyl mode in the CPD lesion, we employed computational models of the Cartesian coordinates and vibrational modes, via DFT calculation using a BLYP functional and a 6-31G* basis set, of a di-thymine CPD dimer. Given that our calculations of thymine and thymidine were consistent with the literature, the applied BLYP/6-31G* method may fairly predict frequencies of the CPD lesion as well. Our equilibrium structures predict that, in the presence of the CPD lesion, both the pyrimidine and cyclobutane rings are nonplanar upon loss of the C5=C6 double bond (Figure 2.1). Furthermore, the puckering of the four-membered cyclobutane ring engenders a nonsymmetric arrangement of the two pyrimidine rings.

The nonsymmetrical configuration of the CPD dimer alters the carbonyl stretching frequencies of the 5' and 3' pyrimidine rings in relation to the pyrimidine monomers. In comparison with thymidine, there is a calculated increase in the net electrostatic potential across the C2=O groups and a net decrease in electrostatic potential of the C4=O groups in the dithymidine CPD dimer (Table 2.3). An inverse linear relationship between the calculated electrostatic potential and ν(C=O) has been observed in myoglobin (*60*). The direction and magnitude of the shift were determined theoretically from two terms involving both the permanent and electric-field-induced dipole moment. For the 5' and 3' thymine rings in the dithymine CPD model, the C2=O stretching frequencies are anticipated at 1761 and 1751 cm^{-1} and C4=O stretching

Table 2.3. Electrostatic Potential Differences. The electrostatic potential of the individual atoms comprising thymine, thymidine, and a di-thymine dimer were calculated using DFT-BLYP/6-31G*. The absolute difference in electrostatic potential was calculated for the different pairs of atoms listed. Values are given in kJ/mol. The numbering of the methyl hydrogen atoms is described in Figure 2.1.

Atom Pairs	Thymine	Thymine CPD		Thymidine
		5'	3'	
C-H modes				
(C6-H)	1.414	0.376	0.862	1.924
(methyl C-H1)	4.028	3.774	3.669	3.598
(methyl C-H2)	4.028	3.811	3.594	3.581
(methyl C-H3)	3.966	3.761	3.464	3.510
C=O and C5-C6 modes				
(C2=O2)	4.066	4.309	4.359	4.175
(C4=O4)	3.711	3.861	3.840	3.924
(C5-C6)	1.473	1.422	0.251	1.406

frequencies at 1712 and 1724 cm^{-1}, respectively (Table 2.4). Comparison of the electrostatic potential with the calculated vibrational modes, along with the inverse relationship reported for stretching frequencies and electrostatic potential, allows tentative assignment of the 1719 cm^{-1} line to the carbonyl groups of the CPD lesion. The higher intensity (strong negative trend) and ~30 cm^{-1} base width demonstrates that it is a combination of many carbonyl modes together.

C-H modes of model compounds and oligonucleotides. The distortion of the DNA modes in the 3000-2800 cm^{-1} spectral window from radiation insult havr been demonstrated previously, but the effect of the radiation and the specific type of DNA lesion formed was not determined (*55*). From our work, it is clear that formation of a CPD lesion introduces steric effects for the C5 methyl groups. This is demonstrated by our tentative assignment of the ν_a(C-H) mode to 2986 cm^{-1} (Table 2.4), a 23 cm^{-1} upshift from the same vibrational mode in thymine and thymidine, and the downshift of ν_s(C-H) relative to the model compound frequencies by up to 15 cm^{-1} in the difference spectra. The vibrational frequencies of these groups may be affected by steric interactions upon base pairing, therefore we focus on the ν(C6-H) modes.

The ν(C6-H) modes are unique because they are located away from positions where base pairing and phosphate linkages occur. Their insular nature to the "normal" chemical interactions of DNA and proximity to the chemical linkage to an adjacent thymine in a CPD lesion makes them candidates for detection and characterization of CPD lesions. The ν(C-H) region of the spectra for the individual bases has been described (*31, 32, 45, 57, 61-65*), but high frequency vibrational modes for DNA

Table 2.4. Experimental and Calculated Vibrational Frequencies of CPD Lesions. Experimentally detected vibrational lines of an *in vitro* CPD from the 8merTT-minus-8merTTCPD difference spectrum are compared to calculated modes to make tentative assignments. Vibrational frequencies of a di-thymidine cyclobutane dimer were calculated using DFT-BLYP/6-31G*. The C-H modes were scaled using a factor of 0.9796. Abbreviations: ν, stretching; ν_a, asymmetric stretching; and ν_s, symmetric stretching.

Mode	Calculated di-Thymine CPD		Experimental Frequency
	5'	3'	
C-H modes[a]			
$\nu_a(CH_3)$	2987	2981	2986
ν(C6-H)	2950	2887	2958
$\nu_s(CH_3)$	2923	2926	2918
C=O and C5-C6 modes[b]			
ν(C2=O)	1761	1751	
ν(C4=O)	1712	1724	1719
ν(C5-C6)	1191	1210	

[a] from Figure 2.4

[b] from Figure 2.3

oligonucleotides have not been well characterized, as vibrational lines in the absorbance spectra (Figure 2.4A and B) are an amalgam of modes from the individual bases. Using difference FT-IR spectroscopy we are able to distinguish the C-H modes of damaged thymine from the contributions of the other nucleotides.

The (C6-H) bonds are not directly affected by dimerization, but conversion of C6 from sp^2 to sp^3 hybridization along with cyclobutane ring formation distorts the C6-H bonds through electronic, mass, and spatial affects. Table 2.4 displays the calculated and experimental frequencies for C-H stretching of different groups. Although the electrostatic potential difference is higher for the methyl-hydrogen atoms (Table 2.3), the proximity of the C6 hydrogen to the electron rich double bond region induces higher bond energy in this group than in the methyl carbon position, demonstrated by the higher frequency vibrational mode. The significant drop in potential difference upon lesion formation, calculated from a di-thymine CPD, reflects the significant shift in ν(C6-H) from greater than 3000 cm^{-1} in thymine and thymidine (Table 2.2) to our tentative assignment of 2958 cm^{-1} in damaged DNA (Table 2.4). This vibrational line is specific to the damaged oligomer and maybe useful as a marker mode for CPD lesions.

The end result of this work is the detection, assignment, and derivation of marker modes in the high (3100 – 2700 cm^{-1}), middle (1800 – 1550 cm^{-1}), and low (1340 – 1200 cm^{-1}) spectral regions. All these modes being independent of one another and resulting from different atom groups provides a redundant system for understanding CPD formation and repair, and allows the extension of this work to other DNA lesions.

ACKNOWLEDGMENTS

We thank Prof. Robert White for generous use of the HPLC instrumentation. This work was supported by American Chemical Society–Petroleum Research Fund (38643-G4 to S.K.), American Cancer Society (IRG-99-225-01 to S.K.), and the Thomas F. and Kate Jeffress Trust (J-613 to S.K.)

REFERENCES

1. Reardon, J. T., and Sancar, A. (2003) *Genes Dev 17*, 2539-2551.
2. Sambrook, J., and Russell, D. W. (2001) pp A2.1, Cold Spring Harbor Laboratory Press, Cold Spring Harbor, New York.
3. Beukers, R., Ylstra, J., and Berends, W. (1958) *Rec Trav Chim Pay B 77*, 729-732.
4. Patrick, M. H., and Rahn, R. O. (1976) in *Photochemistry and Photobiology of Nucleic Acids* (Wang, S. Y., Ed.) pp 35-95, Academic Press, New York.
5. Douki, T., Court, M., and Cadet, J. (2000) *J Photochem Photobiol B 54*, 145-154.
6. You, Y. H., Lee, D. H., Yoon, J. H., Nakajima, S., Yasui, A., and Pfeifer, G. P. (2001) *J Biol Chem 276*, 44688-44694.
7. Chinnapen, D. J., and Sen, D. (2004) *Proc Natl Acad Sci U S A 101*, 65-69.
8. Liu, F.-T., and Yang, N. C. (1978) *Biochemistry 17*, 4865-4876.
9. MacFarlane, A. W., and Stanley, R. J. (2001) *Biochemistry 40*, 15203-15214.
10. Taylor, J.-S., and Brockie, I. R. (1988) *Nuc Acids Res 16*, 5123-5136.
11. Kim, S. T., and Sancar, A. (1991) *Biochemistry 30*, 8623-8630.
12. Sancar, G. B., Smith, F. W., Reid, R., Payne, G., Levy, M., and Sancar, A. (1987) *J Biol Chem 262*, 478-485.
13. Husain, I., Griffith, J., and Sancar, A. (1988) *Proc Natl Acad Sci U S A 85*, 2558-2562.
14. Park, H., Zhang, K., Ren, Y., Nadji, S., Sinha, N., Taylor, J. S., and Kang, C. (2002) *Proc Natl Acad Sci U S A 99*, 15965-15970.
15. Camerman, N., and Camerman, A. (1970) *J Am Chem Soc 92*, 2523-2527.

16. Camerman, N., and Camerman, A. (1968) *Science 160*, 1451-1452.

17. McAteer, K., Jing, Y., Kao, J., Taylor, J. S., and Kennedy, M. A. (1998) *J Mol Biol 282*, 1013-1032.

18. Taylor, J. S., Garrett, D. S., Brockie, I. R., Svoboda, D. L., and Telser, J. (1990) *Biochemistry 29*, 8858-8866.

19. Sanders, D. B., and Wiest, O. (1999) *J Am Chem Soc 121*, 5127-5134.

20. Schmitz, M., Tavan, P., and Nonella, M. (2001) *Chem Phys Lett 349*, 342-348.

21. Vande Berg, B. J., and Sancar, G. B. (1998) *J Biol Chem 273*, 20276-20284.

22. Deering, R. A., and Setlow, R. B. (1963) *Biochim Biophys Acta 68*, 526-534.

23. Mori, T., Nakane, M., Hattori, T., Matsunaga, T., Ihara, M., and Nikaido, O. (1991) *Photochem Photobiol 54*, 225-232.

24. Gallagher, S. (1996) *Immunoblot Detection*, Vol. 1, Supplement 4 ed., John Wiley & Sons, New York.

25. Nakane, P. K. (1968) *J Histochem Cytochem 16*, 557-560.

26. Kim, S., and Barry, B. A. (2001) *J Phys Chem B 105*, 4072-4083.

27. Aida, M., Kaneko, M., Dupuis, M., Ueda, T., Ushizawa, K., Ito, G., Kumakura, A., and Tsuboi, M. (1997) *Spectrochim Acta 53*, 393-407.

28. Colarusso, P., Zhang, K., Guo, B., and Bernath, P. (1997) *Chem Phys Lett*, 39-48.

29. Florian, J., and Hrouda, V. (1993) *Spectrochim Acta 49A*, 921-938.

30. Graindourze, M., Smets, J., Zeegers-Huyskens, T., and Maes, G. (1990) *J Mol Struct 222*, 345-364.

31. Mathlouthi, M., Seuvre, A.-M., and Koenig, J. (1983) *Carbohyd Res 122*, 31-47.

32. Mathlouthi, M., Seuvre, A.-M., and Koenig, J. (1984) *Carbohyd Res 134*, 23-28.

33. Les, A., Adamowicz, L., Nowak, M., and Lapinski, L. (1992) *Spectrochim Acta 48A*, 1385-1395.

34. Szczepaniak, K., Szczesniak, M. M., and Person, W. B. (2000) *J Phys Chem A 104*, 3852-3862.

35. Zhang, S. L., Michaelian, K. H., and Loppnow, G. R. (1998) *J Phys Chem A 102*, 461-470.

36. Aamouche, A., Ghomi, M., Coulombeau, C., Grajcar, L., M.H., B., Jobic, H., and Berthier, G. (1997) *J Phys Chem A 101*, 1808-1817.

37. Letellier, R., Ghomi, M., and Taillandier, E. (1987) *Eur Biophys J 14*, 423-430.

38. Letellier, R., Ghomi, M., and Taillandier, E. (1987) *J Biomol Struct Dyn 4*, 663-683.

39. McNutt, A., Haq, S., and Raval, R. (2002) *Surf Sci 502-503*, 185-192.

40. Nowak, M. J. (1989) *J Mol Struct 193*, 35-49.

41. Rush III, T., and Peticolas, W. L. (1995) *J Phys Chem 99*, 14647-14658.

42. Susi, H., and Ard, J. S. (1974) *Spectrochim Acta 30A*, 1843-1853.

43. Tsuboi, M., Komatsu, M., Hoshi, J., Kawashima, E., Sekine, T., Ishido, Y., Russell, M. P., Benevides, J. M., and Thomas Jr, G. J. (1997) *J Am Chem Soc 119*, 2025-2032.

44. Tsuboi, M., Takeuchi, Y., Kawashima, E., Ishido, Y., and Aida, M. (1999) *Spectrochim Acta A 55*, 1887-1896.

45. Tsuboi, M. (1969) *Appl Spectrosc Rev 3*, 45-90.

46. Jorns, M. S., Sancar, G. B., and Sancar, A. (1985) *Biochemistry 24*, 1856-1861.

47. Dohy, D., Ghomi, M., and Taillandier, E. (1989) *J Biomol Struct Dyn 6*, 741-754.

48. Ghomi, M., Letellier, R., and Taillandier, E. (1990) *J Mol Struct 238*, 55-69.

49. Taillandier, E., Liquier, J., and Taboury, J. A. (1985) in *Advances in Infrared and Raman Spectroscopy* (Clark, R. J. H., and Hester, R. E., Eds.) pp 65-114, John Wiley & Sons, Chichester.

50. Ghomi, M., Letellier, R., Liquier, J., and Taillandier, E. (1990) *Int J Biochem 22*, 691-699.

51. Guan, Y., Choy, G. S.-C., Glaser, R., and Thomas Jr, G. J. (1995) *J Phys Chem 99*, 12054-12062.

52. Guan, Y., and Thomas Jr, G. J. (1996) *Biopolymers 39*, 813-835.

53. Seuvre, A.-M., and Mathlouthi, M. (1987) *Carbohyd Res 169*, 83-103.

54. Liquier, J., and Taillandier, E. (1996) in *Infrared Spectroscopy of Biomolecules* (Mantsch, H. H., and Chapman, D., Eds.) pp 131-158, Wiley-Liss, New York.

55. Dovbeshko, G. I., Gridina, N. Y., Kruglova, E. B., and Pashchuk, O. P. (2000) *Talanta 53*, 233-246.

56. Aleksanyan, V. T., and Antipov, B. G. (1982) *Theochem - J Mol Struc 6*, 15-24.

57. Ivanov, A. Y., Krasnokutski, S. A., Sheina, G., and Blagoi, Y. P. (2003) *Spectrochim Acta A Mol Biomol Spectrosc 59*, 1959-1973.

58. Weinblum, D., and Johns, H. E. (1966) *Biochim Biophys Acta 114*, 450-459.

59. Cárdenas, G. I., Figueroa, K. A., Vargas C., V., Gómez-Jeria, J. S., and Campos-Vallette, M. M. (1988) *Spectrosc Lett 21*, 107-125.

60. Phillips, G. N., Teodoro, M. L., Li, M. L., Li, T., Smith, B., and Olson, J. S. (1999) *J Phys Chem B 103*, 8817-8829.

61. Mathlouthi, M., and Seuvre, A.-M. (1986) *Carbohyd Res 146*, 15-27.

62. Mathlouthi, M., Seuvre, A.-M., and Koenig, J. (1984) *Carbohyd Res 131*, 1-15.

63. Mathlouthi, M., Seuvre, A.-M., and Koenig, J. (1986) *Carbohyd Res 146*, 1-13.

64. Leulliot, N., Ghomi, M., Jobic, H., Bouloussa, O., Baumruk, V., and Coulombeau, C. (1999) *J Phys Chem B 103*, 10934-10944.

65. Fritzsche, H. (1967) *Biochim Biophys Acta 149*, 173-179.

CHAPTER III

Tryptophanyl Radical Formation

During DNA Repair by Photolyase

ABSTRACT

Photolyase catalyzes the repair of cyclobutane pyrimidine dimer (CPD) type lesions in DNA. Repair is the consequence of an electron transfer event from the photoactive chromophore $FADH^-$ to the CPD lesion. Although previous work using biochemical and theoretical techniques have identified amino acid residues necessary for efficient catalysis, the mechanism of electron transfer has not been elucidated fully. Using difference FT-IR spectroscopy to monitor laser-flash induced photorepair, we have identified vibrational modes indicative of the formation of semiquinone FAD and a tryptophanyl radical. These results support the hypothesis that electron transfer to pyrimidine dimers occurs via an indirect electron transfer event from the isoalloxazine moiety of the FAD cofactor through a tryptophan intermediate to the dimer.

Discovery of a tyrosyl radical as the essential organic electron donor in ribonucleotide reductase (*1*) changed the paradigm of proteins as mere structural elements in enzymatic reactions. This finding introduced the concept of protein-mediated electron transfer from amino acid radical species. Tyrosyl radicals are the most studied of the amino acid radical types, but radical species of glycine, cysteine, and tryptophan have also been identified (*2*). Tryptophan is unique among the radical forming amino acids in that it can form both neutral and cationic species depending on the pH of the local environment (*3*). The enzyme DNA photolyase has been shown to be a model for tryptophan radical formation and electron transfer, displaying activity as a single cofactor, single subunit entity.

The DNA repair enzyme, photolyase, is capable of two distinct light driven electron transfer (ET) events: photoactivation and photorepair. Photoactivation is the light driven reduction of the FADH• cofactor to the reduced state by the transfer of electrons through a chain of aromatic amino acid radicals (*4, 5*). The biologically important photorepair process (Figure 3.1A) is the light driven catalytic reversal of thymine dimers to their monomeric form. The photorepair process has been examined using site directed mutagenesis of active site residues (*6, 7*), ultra-fast UV-Vis spectroscopy (*8, 9*), and molecular modeling techniques (*10-13*) with mixed results. It has been determined that active-site tryptophan residues interact with the pyrimidine dimer, and that the distance from the catalytic cofactor to the CPD lesion may require an intermediate for electron transfer.

To investigate the photorepair process and determine if radical formation occurs, we have employed the difference FT-IR technique. The advantage of our experimental

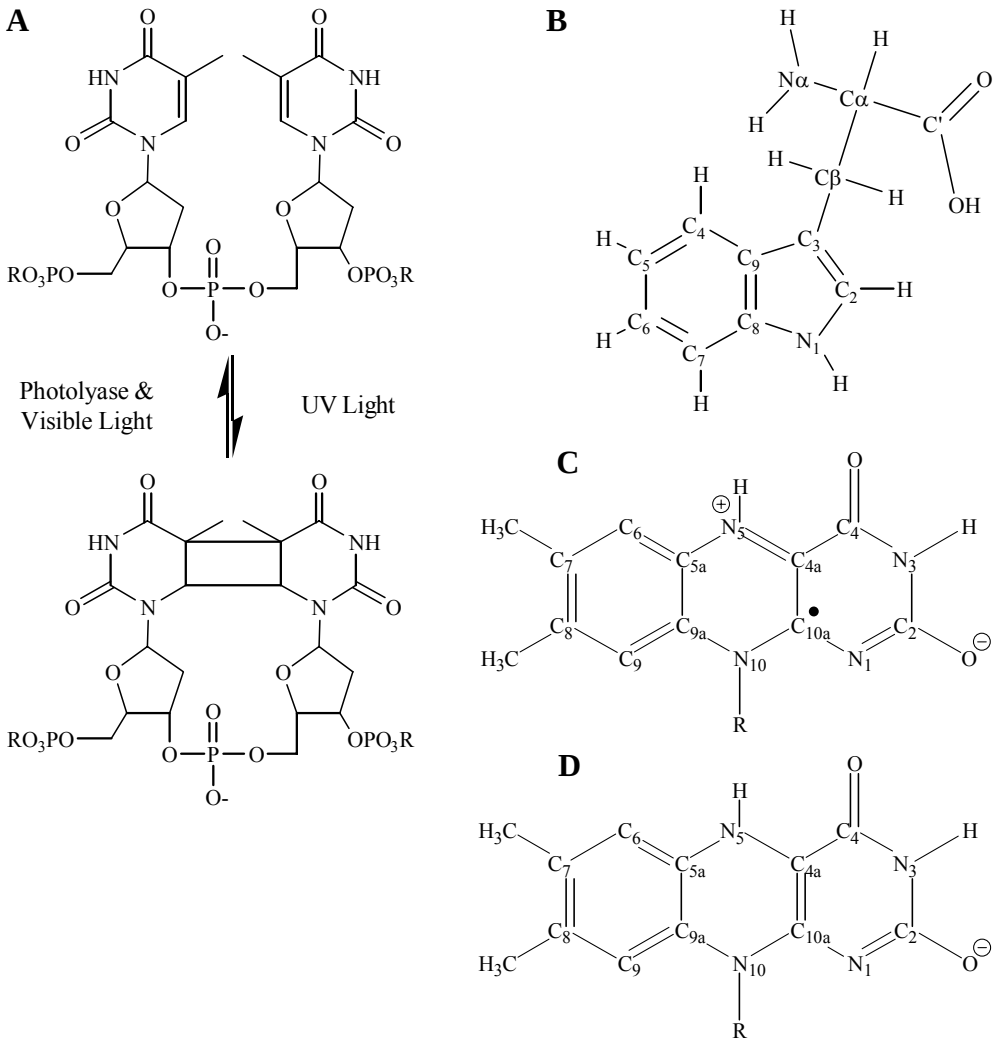

Figure 3.1. The Photorepair Scheme and Molecular Structures. (A) The DNA damage and repair cycle. In the presence of UV light, adjacent pyrimidines will dimerize to form a cyclobutane pyrimidine dimer. Photolyase catalyzes the reversion of dimers to monomeric form in the presence of light. (B) Structure and numbering system for tryptophan. The isoalloxazine portion of FAD is shown in the (C) neutral radical and (D) 1-electron reduced form.

design derives from the exquisite sensitivity of FT-IR to changes in molecular bonds that occur during electron transfer and repair of CPD lesions, allowing us to monitor the reaction as it proceeds with broad sensitivity to enzyme, cofactor, and substrate reactions simultaneously. We have purified *E. coli* photolyase and using laser pulse stimulation, generated light-minus-dark difference spectra of the photorepair process. We observed the first experimental evidence of amino acid radical formation during the photorepair process.

Verification of radical formation was obtained using isotopically labeled tryptophan which, upon generation of photorepair difference spectra, display significant vibrational line shifts. Because only tryptophan sidechains were modified, the shift in observed modes can only be attributable to reactive tryptophan species involved in the repair process. We have tentatively assigned vibrational modes due to ground state amino acids and radical formation in the enzyme during DNA repair and compared these with published values.

EXPERIMENTAL PROCEDURES

Protein expression and purification. Our bacterial expression of photolyase employed the *E. coli* strain CSR603 F' lacI^{Q} containing the photolyase expression plasmid pMS969 (*14*), a generous gift from Prof. Aziz Sancar (UNC Chapel Hill, NC). Starting with dilution of an overnight culture of CSR603 F' lacI^{Q} with pMS969 grown in LB and 50 μg/mL ampicillin, wildtype photolyase expression was induced with isopropylβ-D-1-thiogalactopyranoside (IPTG) to a final concentration of 1 mM when OD_{600nm} of ~0.5 was obtained. After 10 hours of growth at 37^{o}C, cultures were harvested by centrifugation at 6,000x*g*, resuspended in buffer A (50 mM HEPES, 50 mM NaCl, 5

mM β-ME, 10% glycerol) at a ratio of 5 mL buffer per gram of cells, and frozen at -80ºC. The typical yield was 3.3 grams of cells per liter of culture.

Protein purification followed the protocols established in (*15-17*), and all steps were conducted at 4ºC. Cells were thawed, and lysed by the French press at ~16,000 psi. Cell debris was cleared by two rounds of centrifugation: 30 min at 25,000x*g*, followed by 1 hour at 120,000x*g*. Ammonium sulfate (43 g/100 mL lysate) was added over a period of one hour, and the solution was stirred for another hour. The material was pelleted by centrifugation for 30 min at 25,000x*g*. The supernatant was discarded and the pellet was resuspended to a volume of 30 mL.

Ammonium sulfate was removed using a 100 mL Biogel P-6 (Bio-Rad, Hercules, CA) column equilibrated with buffer A. Protein-containing fractions from the Bio-Gel P-G column were then loaded onto a Blue Sepharose column (Amersham Biosciences, Piscataway, NJ), equilibrated with buffer B (25 mM HEPES, 100 mM KCl, 5 mM β-ME, 10% glycerol), and photolyase was eluted with buffer C (buffer B with 500 mM KCl). Blue-colored fractions, due to the presence of the flavosemiquinone in photolyase, diluted fivefold with buffer D (25 mM HEPES, 5mM β-ME, 10% glycerol) to lower the salt concentration, were subsequently applied to a Heparin Sepharose column (Amersham Biosciences) in buffer B, and photolyase was eluted with buffer C. Blue-colored fractions were combined and analyze using UV-vis spectroscopy to determine the concentration of photolyase by its characteristic peaks at 380, 580, and 633 nm (*18, 19*). Photolyase was concentrated using Amicon C-30 concentrator (Millipore, Billerica, MA), and photolyase was exchanged into buffer B using Econo-Pac 10DG columns (Bio-Rad). Glycerol was added to the photolyase samples at a final concentration of 30%. The

concentrated protein was analyzed by Coomassie-stained SDS-PAGE (*20*) and determined to be greater than 95% pure. Purified photolyase was snap frozen in liquid nitrogen, and stored at -80ºC until use.

Isotopic labeling of photolyase. Photolyase with $^2H_5$-tryptophan was also purified for the studies herein. Obtained from the Yale Genetic Stock Center, the tryptophan auxotroph strain PLK983 (*21*) was transformed with pMS969 and pMS421 (*22*), expressing $lacI^Q$ (a generous gift from Prof. Timothy Larson (Virginia Tech, VA). A single colony was inoculated in defined medium (*21, 23-25*): 12.8 g $Na_2HPO_4 \cdot 7H_2O$, 3 g KH_2PO_4, 0.5 g NaCl, 1 g NH_4Cl, 493 mg $MgSO_4 \cdot 7H_2O$, 14.7 mg $CaCl_2 \cdot 2H_2O$, 10 g maltose, 41.6 mg Na_2EDTA, 3.15 mg $FeCl_3$, 6.3 µg $Na_2MoO_4 \cdot 2H_2O$, 22 µg $ZnSO_4 \cdot 7H_2O$, 10 µg $CoCl_2 \cdot 6H_2O$, 180 µg $MnCl_2 \cdot 4H_2O$, 9.8 µg $CuSO_4 \cdot 5H_2O$, 0.5 µg vitamin B_{12}, 0.05 µg biotin, 100 µg thiamine HCl, 20 mg methionine, 20 mg leucine, 20 mg histidine, 20 mg threonine, 6 mg uracil, 2.5 mg tryptophan per liter. The overnight culture was diluted into the same medium with $^2H_5$-tryptophan (tryptophan-2',4',5',6',7'–^2H, >97% purity, Isotec, Miamisburg, OH); when the OD_{600nm} reached 0.4 at 37ºC, IPTG was added to 1 mM. After 12 hours of growth, cells were harvested, and labeled cell cultures were purified as above.

Mass Spectral Analysis of Label Incorporation. Incorporation of $^2H_5$-tryptophan into the photolyase enzyme was examined using a combined mass spectrometry / HPLC technique (*26*). Briefly, the purified enzyme is base-hydrolyzed to preserve the integrity of tryptophan residues. The hydrolysate is then derivitized to phenyl isothiocyanate. The mixture is separated by HPLC, and peak fractions were analyzed by mass spectrometry to determine extent of labeling.

Photorepair Substrate. To generate CPD lesion in an 8-base oligonucleotide(*9, 27*), 1.5 mL of 195 μM oligomer DNA in 75 mM potassium phosphate buffer pH 6.8 was degassed with nitrogen in stoppered quartz cuvettes (Starna, Atascadero, CA). Acetone (50 μL) and acetophenone (final concentration 5 mM) were added through a septum. The mixture was then irradiated with UV-B light (312 nm peak output, Spectronics, Westbury, NY) through a polystyrene Petri dish at 4ºC for 3 hours. The resulting 8merTT/8merTTCPD mixture was then lyophilized to remove acetone and acetophenone, and the damaged and non-damaged DNA were separated using HPLC as above. The concentration of the oligonucleotide was determined by UV-vis spectroscopy using an extinction coefficient of 90,000 M^{-1} cm^{-1} at 260 nm with the sequence GAAT<>TAAG (*25, 28*).

Assay. In UV-vis spectrophotometeric assays measuring photorepair *(29)*, the substrate oligonucleotide was diluted with buffer (25 mM Tris pH 7.2, 25 mM NaCl, 1mM EDTA) to a concentration of 9 μM. The solution was degassed for 10 minutes under nitrogen in stoppered quartz cuvettes, prior to the addition of photolyase at a final concentration of 0.75 μM. This mixture was measured in a Shimadzu 2101 UV-vis Spectrophotometer (Shimadzu Scientific Instruments, Columbia, MD) and was utilized as the zero line and is the data point at T=0 min. After every 2 minute interval of illumination with a blacklight source (GE F15T8 BLB) placed 5 cm from the cuvette, a spectrum was recorded. The total time for blacklight illumination was 20 min.

Vibrational spectroscopy. Note that all vibrational data shown herein are averages of at least three experiments, and were analyzed using IGOR Pro (Wavemetrics, Lake Oswego, OR). Infrared experiments were performed using a MCT/A detector in a

Bruker IFS 66v/s infrared spectrometer under vacuum and at room temperature. Spectral conditions were: double-sided, forward-backward acquisition mode, Happ-Genzel apodization function, 20 kHz mirror velocity, 200 scans per interferogram, 1 level of zero filling, and gain of 1. When appropriate, laser illumination was from an Nd:YAG Surelite Continuum laser (Santa Clara, CA) with 355 nm excitation, ~160 mJ per flash, with pulse duration of 6 ns.

Model Compounds. In order to demonstrate vibrational mode shifts upon deuteration of tryptophan, the IR spectra of both natural abundance and $^{2}H_{5}$-tryptophan were obtained. Natural abundance tryptophan (>99% purity) was obtained from Fluka Chemical Corp. (Milwaukee, WI). Tryptophan-2',4',5',6',7'–^{2}H (>97% purity) was obtained from Isotec (Miamisburg, OH), and both compounds were used without further purification. Samples were mulled with potassium bromide (approximately 1 mg sample per 80 mg KBr) using an agate mortar and pestle. The sample crystal was formed in a 7 mm die set with pressure applied using a hand press (Buck Scientific, Norwalk, CT) until a transparent pellet was formed. For FTIR spectroscopy, 200 scans at 2 cm^{-1} resolution were collected for each interferogram, which was 158 s in duration.

Biological difference FT-IR spectra. Prior to infrared measurements, 100 µL of a 157µM *E. coli* photolyase solution was diluted with 500 µL buffer G (10 mM HEPES pH 7.2, 10 mM NaCl, 0.2 mM EDTA) to minimize glycerol contributions, and concentrated using an Amicon C-30 Centricon to 400 µM. The dark blue sample was used immediately. For difference spectra in the absence of DNA, a 10 µL sample of 400 µM photolyase, diluted 1:1 with sterile water, was partially dehydrated on a CaF_2 window under a stream of nitrogen, sandwiched with another CaF_2 window, and held fixed in the

spectrometer using the demountable cell holder. For the difference IR spectra in the presence of damaged DNA, each spectral sample contained 8merTTCPD DNA and photolyase, both at 200 μM.

For each protein sample, one spectrum was recorded before (I_o) and after illumination (I). An Nd:YAG Surelite Continuum (Santa Clara, CA) laser with 355 nm excitation was utilized to initiate light dependent reactions. The laser energy output was ~160 mJ per flash, with pulse duration of 6 ns. Light state spectra were obtained immediately after excitation by five laser flashes. Difference, or light-minus-dark, spectra were constructed by calculating the ratio $-\log(I/I_o)$. Three successive light-minus-dark spectra were recorded and averaged for each sample. Prior to the first illumination, three control, or dark-minus-dark, spectra were recorded and averaged for each sample. Difference spectra were corrected to equal protein content using the amide II absorbance and/or total protein content of individual samples. Double difference spectra were generated by subtracting the photoactivation spectrum from the photorepair spectrum, and a smoothing level of 2 was applied using a binomial algorithm.

RESULTS

Mechanistic proposals for DNA repair by photolyase are principally derived from crystallographic studies of the enzyme in the ground state and in the absence of substrate. However, positive experimental support for these hypotheses has remained elusive, as protonation structures and hydrogen-bonding interactions of amino acid side chains are not well resolved by crystallography. To obtain such information, vibrational spectroscopy, which directly detects chemical bonds and molecular interactions, is one of the most powerful methods. Our aim in this study is the generation of direct

experimental observation of structural changes in the active site of photolyase upon introduction of an *in vitro* substrate. Furthermore, efforts toward obtaining data on model compounds are required, and are detailed below.

Enzyme Purification and Assay. Using published methods (*15-17*), bacterial photolyase was readily purified to near homogeneity, as evidenced by the single band of appropriate molecular mass of 54 kDa in the SDS-PAGE (Figure 3.2A, lane 1). Photolyase was also isolated from a tryptophan auxotroph grown in a medium supplemented with $^{2}H_5$-tryptophan. In this manner, purified photolyase containing isotopically labeled tryptophan was obtained (Figure 3.2A, lane 3). Mass spectral analysis has not been completed, but all of the tryptophans in the protein are expected to have isotope incorporation based on the usage of a tryptophan auxotrophic strain for protein production.

To test the DNA repair activity of our enzyme, we employed a UV spectroscopic method developed initially for use with oligothymidylates to assay enzymatic parameters (*29*). This assay is predicated on the approximately 350-fold decrease (*28*) in extinction coefficient at 260 nm of thymidine upon CPD lesion formation. In the presence of photolyase, an appropriate increase in 260 nm absorbance as a function of time demonstrates that there is complete substrate turnover of 8merTTCPD (Figure 3.2B, filled diamonds). The specific activity was determined to be ~2 dimers/molecule photolyase/min, comparable with published values (*14*). In addition, control reactions were performed in the absence of light (Figure 3.2B, open triangles) or in the absence of damaged DNA (Figure 3.2B, open diamonds). In the absence of light, there is no net increase in absorbance because the enzyme is unable to repair DNA damage in the

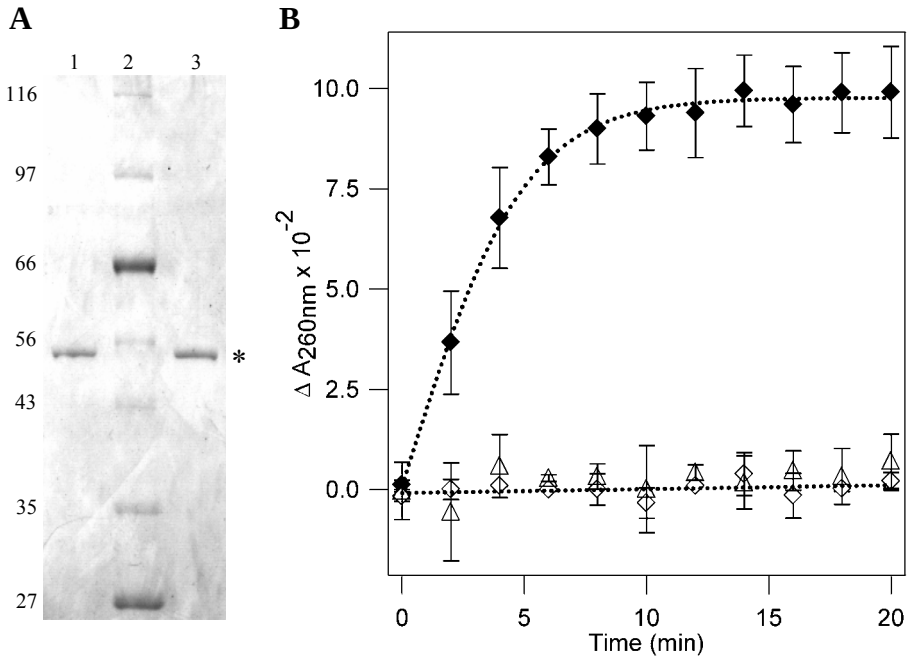

Figure 3.2 Photolyase Gel and Assay. (A) Coomassie-stained SDS-PAGE of (1) wildtype photolyase, (2) molecular weight markers (New England Biolabs, Beverly, MA), and (3) $^{2}H_5$-tryptophan labeled, wildtype photolyase. (B) UV-vis spectrophotometric assay of CPD repair. Samples containing photolyase (0.75 μM) and 8merTTCPD (9 μM) are combined and incubated in either the presence (filled diamonds) or absence (open triangles) of photoreactivating light. Also shown is photolyase and non-irradiated 8merTT incubated with photoreactivating light (open diamonds) as a control. Each trace is an average of three experiments with error bars representing one standard deviation.

absence of light. Similarly, there was no net increase in absorbance when the assay mixture contained non-damaged DNA. From these data, we conclude that pure, active photolyase and artificial substrate have been generated for our spectroscopic studies.

Vibrational spectra of model compounds: isotopomers of tryptophan. For reference, we have obtained experimental IR spectra (Figure 3.3A) of natural abundance L-tryptophan in the ground state (Figure 3.1B), as well as those of $^{15}N_2$-tryptophan (Figure 3.3B, solid line) and of $^{2}H_5$-tryptophan (Figure 3.3C, solid line). The L-tryptophan spectra exhibit excellent signal-to-noise, and compare well with published spectra(*30*). There are four major spectral features at 1667, 1590, 1457, 1415, and 1358-1340 cm^{-1} (Figure 3.3A) in the tryptophan spectrum. These peaks are broad, and contain contributions from multiple modes, as evidenced by the presence of discernable shoulders and other subfeatures. The vibrational mode assignments of the model compound spectra follow those previously reported for 3-methylindole(*31*), with the addition of modes for the peptide portion of the molecule. These include contributions from the Nα-H_2 scissoring mode at 1667 cm^{-1} and asymmetric O-C-O stretching mode at 1590 cm^{-1} in the infrared spectrum of tryptophan (Figure 3.3A and Table 3.1). However, the majority of the tryptophan vibrational lines between 1550-1100 cm^{-1} derive from the benzyl and pyrrole rings (Table 3.1), and therefore should compare well with the vibrational lines of 3-methylindole (*31*). Tentative assignments of key vibrational frequencies for all three isotopomers of tryptophan are included in Table 3.1.

The ^{15}N labeling of tryptophan was expected to shift vibrational lines for modes to which the Nα atom in the peptide amino group and the N1 atom of the pyrrole ring

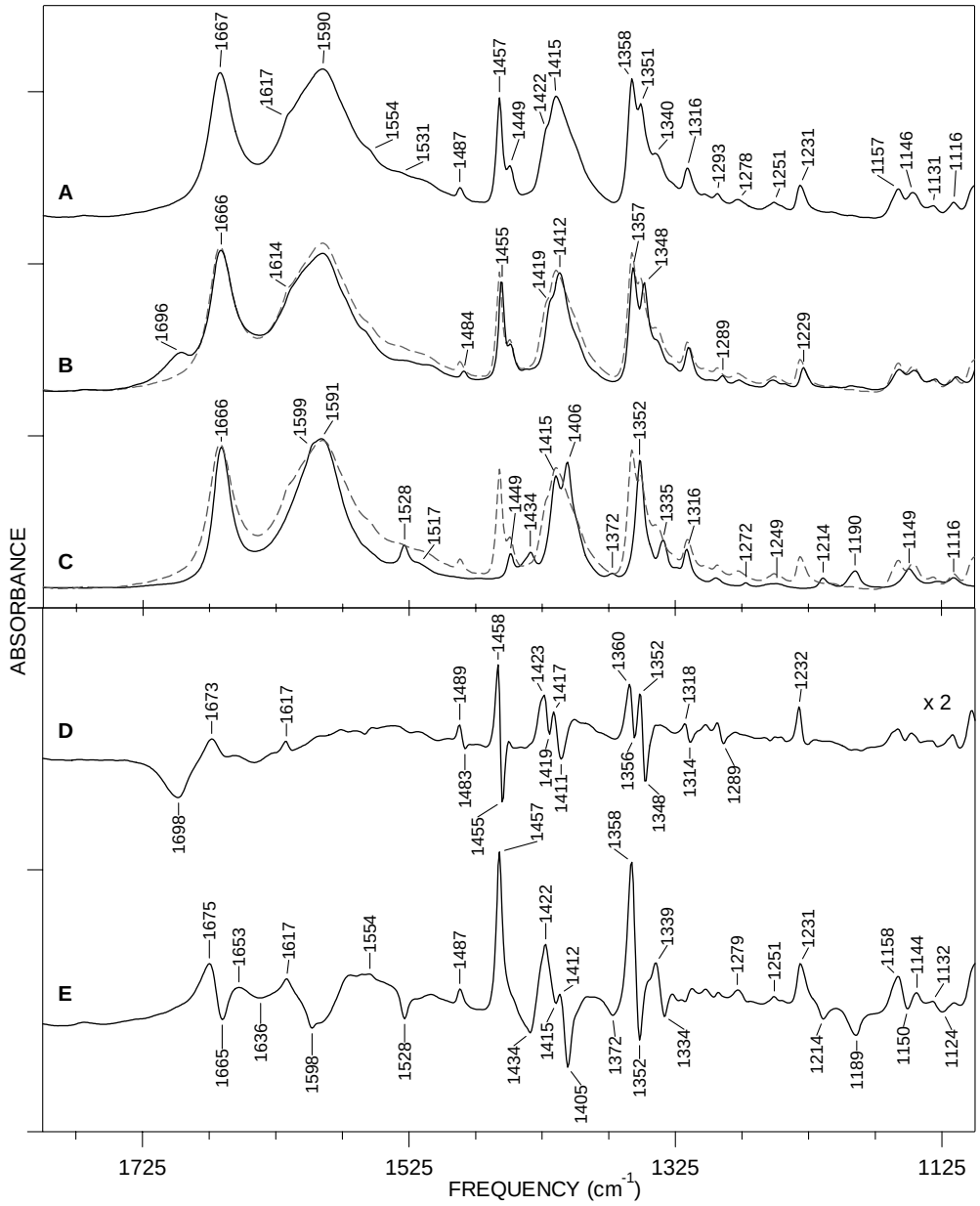

Figure 3.3 FT-IR Absorbance Spectra of Tryptophan and Two of Its Isotopomers. The 1800-1100 cm^{-1} region of infrared spectra of (A) natural abundance, (B) $^{15}N_2$-tryptophan (solid line), and (C) $^{2}H_5$-tryptophan (solid line). To facilitate comparison, the absorbance spectrum of natural abundance tryptophan is shown as a dashed line in (B) and (C). Also shown are isotope-edited, difference spectra of (D) ^{14}N-minus-$^{15}N_2$ tryptophan and (E) ^{1}H-minus-$^{2}H_5$ tryptophan. Spectrum in (D) has been multipled by a factor of two. Tick marks denote 0.4 absorbance units for the y-axis.

Table 3.1. Tentative Vibrational Mode Assignements of Key Modes in L-Tryptophan, $^{15}N_2$-Tryptophan, and $^{2}H_5$-Tryptophan. Averages of three independent spectra of each of the model compounds in KBr pellets were obtained; the frequency of infrared lines from the experimentally determined spectra are presented. Vibrational mode assignments are based on isotope-edited studies of indole (*32, 33*) and computational studies of 3-methylindole (*31*). Abbreviations: ν, stretching; ν_a, asymmetric stretching; δ, bending; sc, scissoring.

Tentative Vibrational Mode Assignment	L-Tryptophan	$^{15}N_2$-Tryptophan	$^{2}H_5$-Tryptophan
sc(Nα-H_2)	1673	1698	1665
ν(C7-C8)	1617	1614	1598
ν_a(O-C-O)	1590	1590	1598
δ(C4-H), δ(C7-H)	1489	1483	1434
δ(C5-H)	1458	1455	1405
δ(C6-H)	1422	1419	1334
ν(C2=C3)	1360/1352	1356/1348	1352
ν(C8-N1), δ(C3-H)	1279	1278	1279

contribute. A band at 1696 cm^{-1} is observed in the $^{15}N_2$-tryptophan spectrum (Figure 3.3B). An isotope-edited, ^{14}N-minus-^{15}N tryptophan spectrum (Figure 3.3D) clearly depicts a 1698 cm^{-1} line upshifted from 1673 cm^{-1} in the ^{15}N labeled compound. Based on group frequency arguments, the 1673 cm^{-1} band in L-tryptophan arose from the NH bending mode of the amino group. We attribute the perturbation of this mode by ^{15}N labeling to conformational alteration or changes in hydrogen bonding. This data would also suggest that ^{15}N labeling of the α-amino group decreases the force constant of the NH_2 bonds.

In comparison to unlabeled tryptophan, components of the major peaks also appear to shift and result in frequencies at 1455, 1412, and 1357-1348 cm^{-1}; weak modes at 1487, 1293, and 1231 cm^{-1} downshift upon ^{15}N labeling to 1484, 1289, and 1229 cm^{-1}, respectively. The corresponding, derivative-shaped spectral bands in this difference spectrum (Figure 3.3D) may have arisen from the expected ^{15}N shifts in the NH rocking, CN stretching, NH wagging, and other coupled vibrational modes. The ^{15}N shifts for these lines are expected to be smaller than the ^{15}N shift for the NH deformation mode of the amino group due to the bonding of the nitrogen to the pyrrole ring.

In contrast, a larger number of distinct spectral alterations are discernable upon deuteration of the indole ring (Figure 3.3C, solid line). This is expected, as isotopic substitution of the benzyl and pyrrole rings will shift frequencies of these functional groups in the 1620-1100 cm^{-1} region of the $^2H_5$-tryptophan spectrum. The narrower lineshape of the broad 1590 cm^{-1} line causes two additional derivatives at (+)1617 / (-)1598 and (+)1554 / (-)1528 cm^{-1} in the ^1H-minus-$^2H_5$ difference data (Figure 3.3E). Isotopic substiution of the indole ring shifts components of the major peaks at 1445,

1412, and 1357-1340 cm^{-1}, and a number of infrared lines are observed in the difference spectrum in the 1460-1200 cm^{-1} region (Figure 3.3E).

Surprisingly, we also observed alteration in the broad 1666 cm^{-1} line in the $^{2}H_{5}$-tryptophan spectrum (Figure 3.3C) which yielded two derivative-shaped features at (+)1675 / (-)1665 and (+)1653 / (-)1636 cm^{-1} in the isotope-edited spectrum (Figure 3.3E). The frequency of these modes preclude their assignment to the indole ring of tryptophan. Thus, the data suggest that infrared lines associated with the terminal amino and carboxylate groups of tryptophan in the ground state are sensitive to isotopic modification of the indole ring.

Inspection of the high frequency region between 3450 and 3350 cm^{-1} corroborated this observation; the isolated, fundamental NH stretches for both the Nα and N1 atoms are expected in this region. A broad line at 3403 cm^{-1} and a shoulder at 3410 cm^{-1} are observed in L-tryptophan (Figure 3.4A). ^{15}N labeling of tryptophan results in 8 cm^{-1} downshift of the band maximum and shoulder to 3395 and 3402 cm^{-1} (Figure 3.4B); the isotope-edited spectrum in this region (Figure 3.4D) has a positive 3412 cm^{-1} and a negative 3393 cm^{-1} line. Noteworthy is the appearance of two distinct bands at 3407 and 3395 cm^{-1} upon ^{2}H labeling of the benzyl and pyrrole rings in tryptophan (Figure 3.4C). The two derivative-shaped features ^{1}H-minus-^{2}H tryptophan spectrum (Figure 3.4E) at (+)3420 / (-)3408 and (+)3401 / (-)3394 cm^{-1} argue that deuteration of the indole ring modifies and abrogates spectral overlap the NH modes of tryptophan.

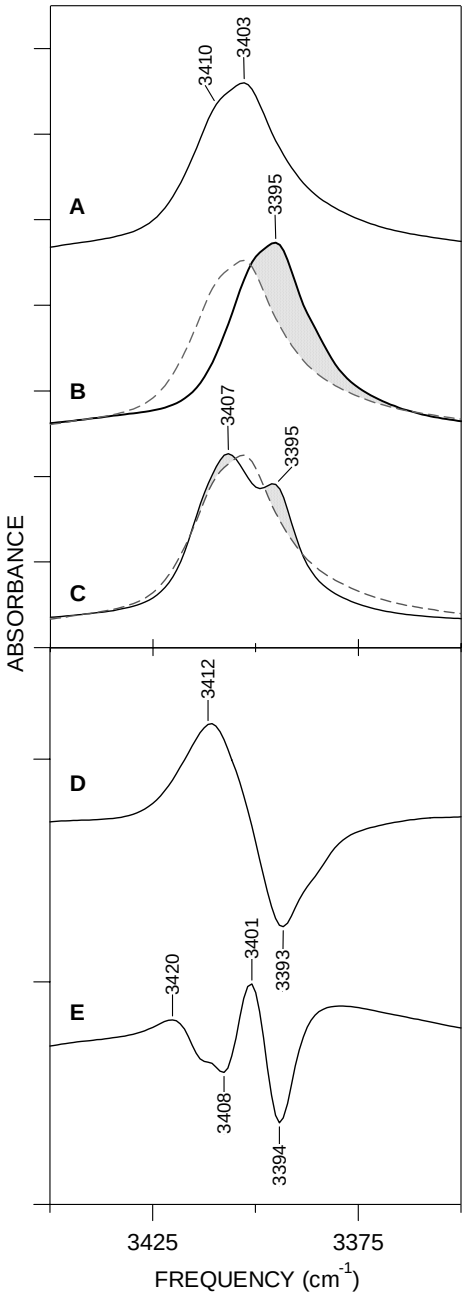

Figure 3.4. High Frequency Modes of Tryptophan Compounds. The 3350-3250 cm^{-1} region of infrared spectra of (A) natural abundance, (B) $^{15}N_2$-tryptophan (solid line), and (C) $^{2}H_5$-tryptophan (solid line). To facilitate comparison, the absorbance spectrum of natural abundance tryptophan is shown as a dashed line in (B) and (C). Also shown are isotope-edited, difference spectra of (D) ^{14}N-minus-$^{15}N_2$ tryptophan and (E) ^{1}H-minus-$^{2}H_5$ tryptophan. Y-axis tick marks 0.2 absorbance units.

We highlight that these results were obtained in the vibrational ground state of the amino acid residue. Taken together, one resultant outcome from the spectroscopic examination of these model compounds is a novel observation of coupling between the indole ring and the terminal groups of tryptophan. Furthermore, the effect of indole deuteration is not equivalent for the force constant of the amino nitrogen and the pyrrole nitrogen atoms.

Photolyase Spectra. Biological absorbance spectra of photolyase before (Figure 3.5A) and after (Figure 3.5B) illumination display vibrational lines characteristic of the peptide backbone. Specifically, the amide I mode, associated with the C=O, exhibits a maximum at 1657 cm^{-1}, and the amide II mode, associated with the coupled N-H/C-N motion, exhibits a maximum at 1547 cm^{-1}. We generated a light-minus-dark difference spectrum (Figure 3.5C, dashed line) to monitor the dynamic changes that occur in photolyase upon transition from the dark, inactive state to light-initiated electron transfer. Positive lines in the difference spectrum reflect perturbations in the protein upon excitation of the flavin cofactor, whereas negative lines arise from structures unique to the dark state of the protein.

As both of the absorbance spectra were acquired in the absence of substrate, the difference data display changes in FAD cofactor (Figure 3.1C and 3.1D) and the photolyase protein during the photoactivation process. There is spectral overlap throughout the 1800-1000 cm^{-1} region from the FAD modes and protein sidechains, such as amino acid radicals formed during the photoactivation process. Given that the extinction coefficient for flavins is higher than those for protein sidechains, we focus first

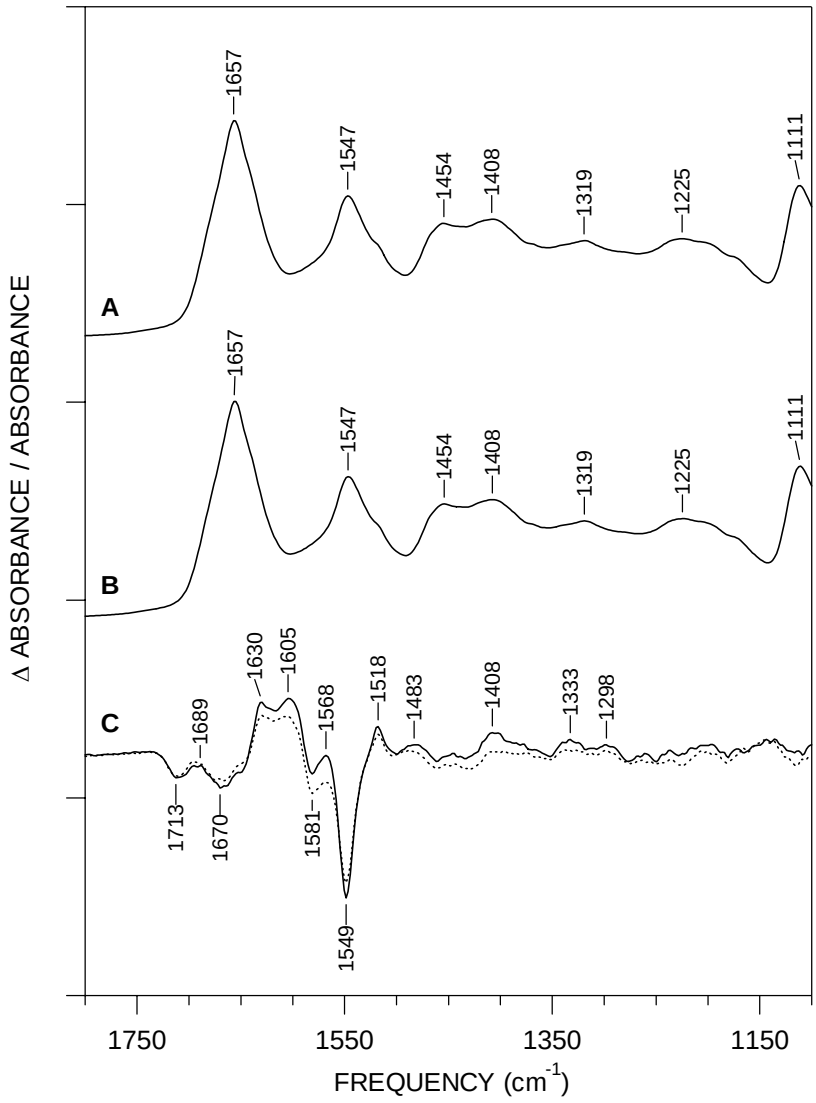

Figure 3.5 FT-IR Spectra of Photolyase. Absorbance spectrum of photolyase (A) before and (B) after illumination. (C) Difference FT-IR spectrum of photolyase in the absence (solid line) and presence (dashed line) of CPD substrate. The difference spectrum is multiplied 1,000-fold to facilitate comparison. Data were acquired at 298K. The y-axis tick marks represent 0.4 absorbance units. Difference spectra were multiplied by 500 for clarity.

on the dominant vibrational lines corresponding to the semiquinone (negative lines) and reduced (positive lines) states of FAD. The vibrational modes arising from FAD oxidation and reduction have been mapped in our laborabory by Lori McKee, and described in the literature (*34*); we utilize these data on model compounds in the analysis of our biological data.

In the 1740-1660 cm^{-1} carbonyl stretching region, a negative infrared lines at 1713 and 1670 cm^{-1} were observed in the photoactivation spectrum (Figure 3.4C). Comparison of the frequency with model compounds begets the interpretation that the 1713 cm^{-1} line can be assigned to the ν(C4=O) and the 1670 cm^{-1} line to the ν(C2=O) of FADH• in photolyase (*34*). Corroborating these assignments are the magnitude of the frequency shifts upon photoreduction (*34*): these modes downshift to 1630 and 1689 cm^{-1}, respectively, in our biological data (Figure 3.5C).

Upon change of redox state, the N_5-C_{4a}-C_{10a}-N_1 region of FAD undergoes rearrangement of single and double bonds, as well as addition of hydrogen. Chemical and structural changes associated with this N_5-C_{4a}-C_{10a}-N_1 region can be measured by infrared methods. Two negative modes at 1581 and 1549 cm^{-1} (Figure 3.5C) correspond well in frequency to the proposed C_{4a}=N_5 and C_{10a}=N_1 motions (*34*), respectively, between rings II and III of the isoalloxazine moiety. Reduction of the photolyase flavin cofactor results in two positive lines at 1605 and 1518 cm^{-1} (Figure 3.5C) that are candidate C_{4a}=C_{10a} and N_5-H/N_1-H modes.

Photorepair Spectra. Toward our experimental goal of measuring changes in the protein environment upon photorepair, we acquired spectra of laser illuminated wild-type (Figure 3.6A) and $^2H_5$-labeled photolyase (Figure 3.6B, solid line) in the presence of

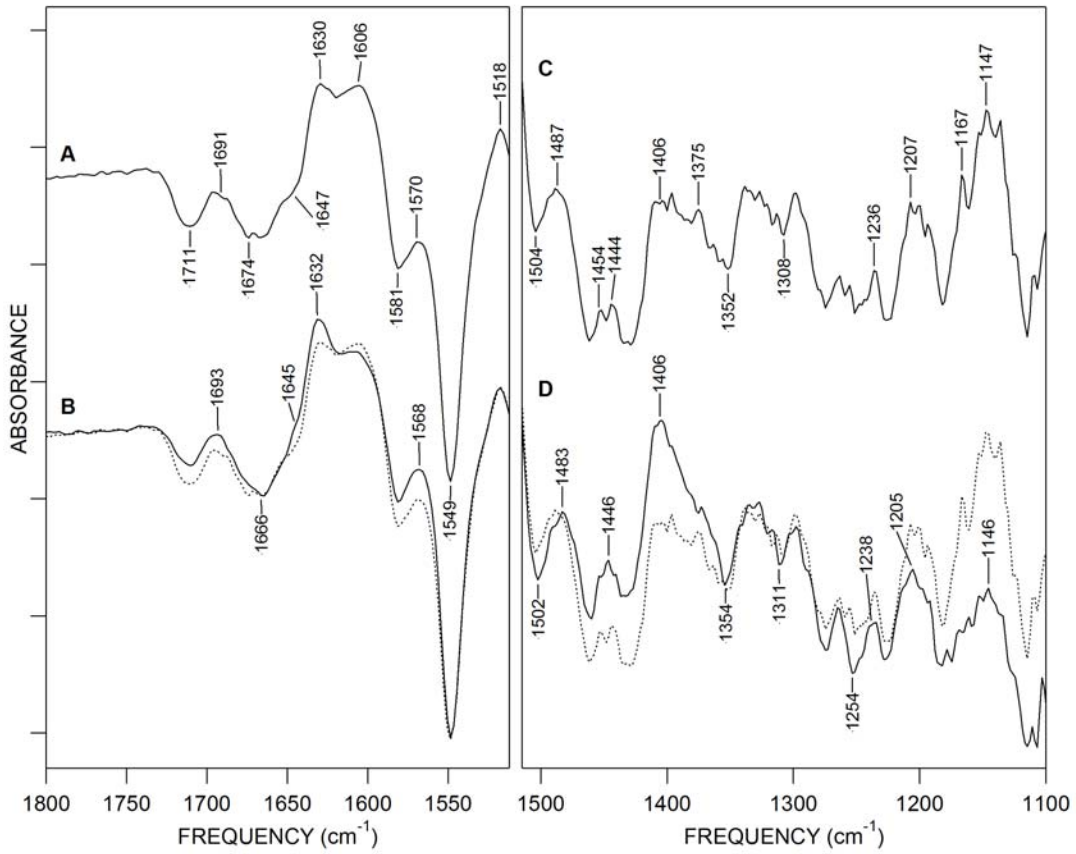

Figure 3.6. Difference Spectra of Photorepair. Difference FT-IR spectra of photolyase in the presence of an 8-base oligonucleotide containing a CPD lesion. Data were acquired on purified photolyase that either are (A, C) unlabeled or (B, D) contain $^{2}H_{5}$-tryptophan (solid line). Spectrum in (A, C) is repeated as a dashed line in (B, D). Data were acquired at 298K. Tick marks on the y-axis are 1 x 10^{-4} absorbance units in the first panel and 1 x 10^{-5} absorbance units in the second panel.

an 8-base oligonucleotide containing a centrally located cyclobutane dimer (described in Chapter II) at room temperature. Selection of the $^{2}H_{5}$-isotopomer for protein labeling was based on mathematical predictions of vibrational frequencies (*31, 35*), the magnitude of shift upon labeling (*32, 33*), and characteristics of the radical species (*23, 35, 36*). These studies cumulatively argue that although ^{15}N-tryptophan may ideally suited for the detection of a shift in δ(N-H) mode in the ground and cation radical states, deuteration of the indole ring will induce larger shifts in vibrational modes and thus can facilitate the detection of cationic species and neutral radical species, which lack a hydrogen at the N1 position. Furthermore, electron spin density is predicted to localize primarily around N1, C2, and C3 in the cation radical and N1 and C2 in the neutral radical, with minor contributions from the C4 and C6 positions in both radical species and C7 in the cationic species (*35, 36*). A significant perturbation of the C2=C3 bond is expected to occur for both radicals, the stretching frequency of which is not expected to be significantly altered from ^{15}N labeling (*32*).

Upon initial inspection of the infrared spectrum of the photorepair reaction (photorepair spectra) using wild-type photolyase (Figure 3.6A), modes attributable to photoreduction FAD can be detected. The carbonyl stretching lines at 1713, 1689, and 1670 cm^{-1} have shifted to 1711, 1691, and 1674 cm^{-1} with introduction of substrate. There are no other significant shifts above 1515 cm^{-1} compared to the photoactivation spectrum (Figure 3.5C). As described by the model compound data, vibrational lines from the tryptophan sidechain are expected below 1500 cm^{-1} (Figure 3.6C). To discriminate the tryptophan modes from those of the protein, cofactor, and substrate comparison to labeled tryptophan must be made.

Introduction of $^{2}H_5$-tryptophan into photolyase alters the frequency of the high frequency lines to 1693, 1666, 1632, and 1568 cm^{-1} (Figure 3.6B), along with a change in intensity at ~1570 cm^{-1}, although incorporation of the label into FAD is not expected. Significant changes in the lower frequency region of the spectrum can be seen by comparison of $^{2}H_5$-tryptophan labeled photolyase (Figure 3.6D, solid line) and wild-type photolyase (Figure 3.6D, dotted line). Shifts in frequency and intensity between 1515 and 1354 cm^{-1} are easily discernable upon deuteration, with a definite increase in intensity apparent at 1406 cm^{-1}. The 1250 to 1100 cm^{-1} region of the spectrum decreases in intensity with label incorporation, the largest decrease occurring at 1147 cm^{-1} in comparison with the wild-type spectrum.

From these difference spectra (Figure 3.6) the contribution of the tryptophanyl sidechain can be detected when shifted by the isotopic label. As flavin modes still predominate the high frequency region of the spectrum, the photoactivation spectrum of wild-type enzyme (Figure 3.5C) was subtracted 1:1 from the photorepair spectrum to remove contributions from the light-driven reduction of FAD. Similar photoactivation spectra were obtained for the $^{2}H_5$-labeled photolyase (data not shown), and subtracted from the photorepair spectrum obtained using $^{2}H_5$-labeled photolyase. The double-difference spectra obtained in this manner are presented in Figure 3.7. The signal-to-noise ratio of these constructions is less than 3.0×10^{-6} AU, allowing us to identify modes related to substrate and possible radical formation in the photorepair process.

Double Difference Spectra of Photorepair. The double difference spectrum of wild type enzyme (Figure 3.7A) displays negative lines at 1714, 1633, 1597 and 1572 cm^{-1} which have contributions from the most prominent negative lines of the 8merTT-

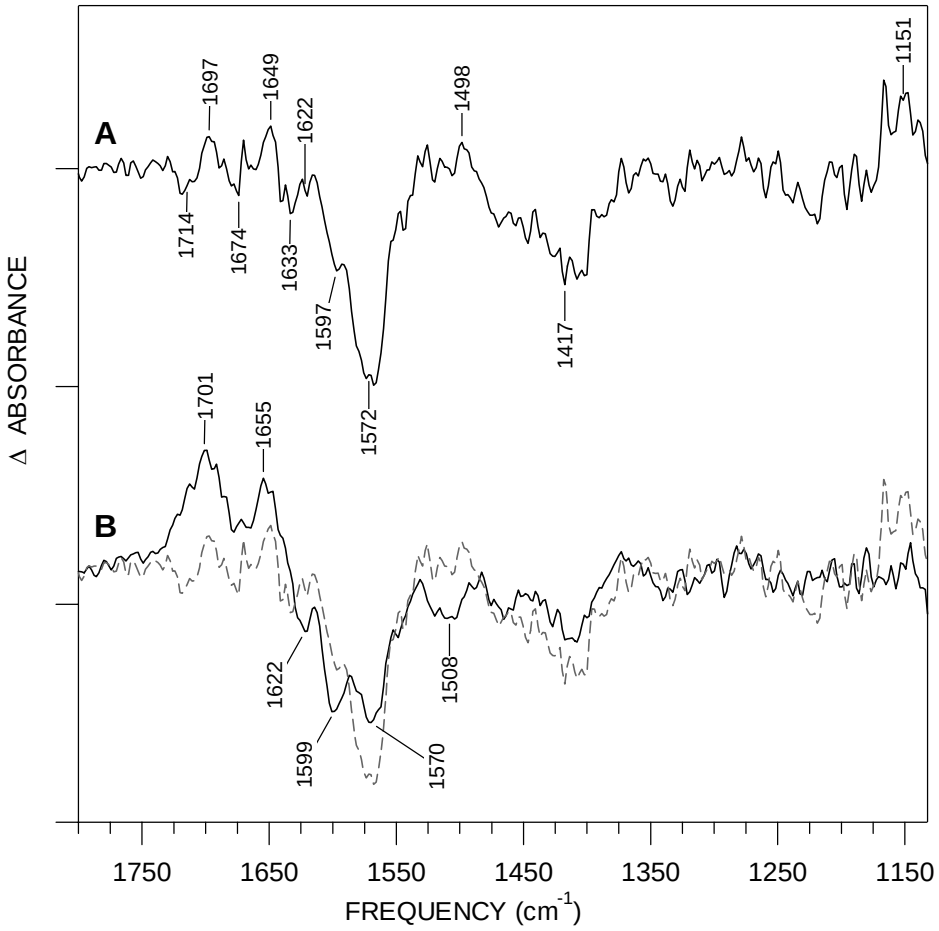

Figure 3.7. Double Difference Spectra of Photorepair. Double-difference FT-IR spectra of photorepair were generated by subtraction of photolyase difference spectrum in the absence of substrate from the photolyase difference spectrum in the presence of substrate. Data shown were acquired from (A) unlabeled, wildtype photolyase and (B) $^{2}H_{5}$-tryptophan labeled photolyase. Spectrum in (A) is repeated as a dashed line in (B). Data were acquired at 298K. Tick marks on the y-axis represent 5 x 10^{-5} absorbance units.

minus-8merTTCPD differnce spectrum (Chapter II, Figure 2.3), and the positive line at 1697 cm^{-1} vibrational line may have some contributions from the positive line in the DNA difference spectrum. Successful catalysis of the repair reaction is evident from this spectrum, indicating that our protein is active under experimental conditions.

Comparison of the double difference spectrum of isotopically labeled (Figure 3.7B, solid line) and wild-type enzyme (Figure 3.7B, dotted line) reveals that there is a decrease in intensity of the 1572, 1498, and 1406 cm^{-1} lines upon labeling. The vibrational lines between 1750 and 1630 cm^{-1}, observable in the wild type double difference repair spectrum, are no longer distinct and have been replaced by strong positive modes at 1701 and 1655 cm^{-1}. Label incorporation also induces an intensity increase of the 1597 cm^{-1} line with a small upshift in frequency to 1599 cm^{-1}. Unique to the isotopically labeled sample is the vibrational line at 1508 cm^{-1}. Conspicuously absence in the labeled-photolyase double difference spectrum is the 1151 cm^{-1} vibrational line.

DISCUSSION

Photolyase enzymes are rich in aromatic amino acids, in particular tryptophan residues. A number of studies implicated that photosensitized repair of pyrimidine dimers could be driven by tryptophan in the absence of a flavin cofactor. It has been demonstrated that the the sole presence of a tripeptide Lys-Trp-Lys catalyzes monomerization of CPD lesions (*37*). In addition, antibodies raised against pyrimidine dimers, which effectively reverse pyrimidine dimers, were shown to contain a photosensitizing tryptophan at the binding site (*38*). These tryptophans were postulated to achieve dimer cycloreversion by electron transfer from a photoexcited tryptophan to

the dimer, yielding a dimer radical anion intermediate that splits into monomers. Given the abundance of tryptophan residues in photolyase, these studies raised the possibility that this residue may participate in splitting the CPD lesion. By monitoring quenching of tryptophan fluorescence by substrate addition, W277 in *E. coli* photolyase was targeted as the sole residue implicated in CPD repair via electron transfer (*6*).

Vibrational spectroscopy can provide novel molecular information about bond orders, conformation, and changes due to the distribution of total electron density throughout the molecule under study. To examine whether tryptophan residue(s) participate in redox reactions during photorepair, our strategy involved use of infrared techniques to first lay the groundwork for recognition of tryptophan modes and, secondly, for following dynamic changes concomitantly in photolyase and substrate under native conformations, instead of conformations stabilized by crystals. The work presented herein focuses on the first application of difference infrared methods in the study of photorepair.

Vibrational spectra of model compounds: isotopomers of tryptophan. The majority of studies in the literature aimed at elucidating tryptophan vibrational modes have focused on the experimental and computational delineation of vibration description of indole (*32, 33*) and 3-methylindole (*31*), which are representative of the tryptophan side chain. Only a few studies examining tryptophan have been reported in the literature (*30, 39*). Given that the amino acid residues has 27 atoms, the 75 vibrational modes of tryptophan are distributed as 51 in-plane vibrations and 24 out-of-plane vibrations. Of these modes, only a small number of these vibrational lines have consistent assignments.

Highlighted in this work are the NH and NH_2 motions of the Trp residue. Given the resolution and signal-to-noise ratio of our data, we conclude that there are two distinct, but overlapping, modes in the 3400 cm^{-1} region of the model compound spectra (Figure 3.4). The 3410 and 3403 cm^{-1} lines are assigned to the N1-H and Nα-H stretches of the tryptophan molecule, respectively, as they both downshift 8 cm^{-1} upon ^{15}N labeling. This interpretation does not support a previous assignment of the 3119 cm^{-1} band to the ν(Nα-H), based on normal coordinate analysis (*30*). The corresponding infrared line at 3116 cm^{-1} in our L-tryptophan spectrum does not shift upon $^{15}N_2$ labeling of the residue (data not shown). The NH_2 scissoring mode normally lies between 1590 and 1650 cm^{-1} in primary aromatic amines. In the work herein, the frequency at 1673 cm^{-1} is assigned to the NH_2 scissoring mode in tryptophan.

Photolyase Spectra. The photorepair process in photolyase offers an opportunity to characterize tryptophan oxidation. Selective isotopic substitution of the tryptophan, which can be achieved in a controlled manner in photolyase, should allow a thorough investigation of the chemical properties of the residue during this electron transfer process. Because we observe negative modes specific to labeled and unlabeled tryptophan in the fingerprint region of the difference spectrum, and positive modes that are shifted in position between the two repair schemes, we propose that a amino acid radical is involved in the photorepair process. The photolyase enzyme does show a propensity toward amino acid radical formation, which has been demonstrated in the light mediated photoactivation process (*5, 16, 23, 40*).

By comparison to calculated vibrational modes for indole radicals (*41*), our data indicate both the cation and neutral radical species may be formed during the photorepair

process. This may be due to the initial formation of the cation radical followed by its deprotonation to the neutral radical state. The indole nitrogen has a pKa of approximately 17, formation of the cation radical lowers the pKa to 4.3 (*3*), allowing the nitrogen to become deprotonated at physiological pH or in the presence of strongly basic species.

Molecular orbital calculations have revealed that the spin density of the tryptophan radical is localized primarily at the C2 and C3 positions in the cation radical and at the C3 and N1 in the neutral radical (*15*). The qualitatively different patterns of spin density distribution predicted for tryptophan radicals indicate that deuteration at the C2 position will affect the spectrum significantly for the cation radical case, but not for the neutral radical. The results of these molecular orbital calculations suggest that it is possible to differentiate between electron versus H-atom transfer experimentally, by examining the spectra of protein samples containing indole-^{15}N and indole-$^{2}H_5$ tryptophans. The infrared spectra of tryptophan and isotopically labeled tryptophan are presented in this work for reference because of the possible involvement of this amino acid in the photorepair process. At first inspection of the model compound difference spectrum, incorporation of the deuterium in the indole ring greatly perturbs the vibrational spectrum. Using this as a guide, we are able to determine that tryptophan plays a role in the photorepair process by comparing spectra obtained on the enzyme with and without the isotopic label.

The frequency of the 1552 cm^{-1} Trp band is known to be sensitive to the torsional chi2 angle of the Cβ-indole bond (*42*). The difference in frequency may be due to a shift of the W3 band of a Trp residue that rotates around the Cβ-indole bond during the

transition. The W3 difference frequency at 1545 cm^{-1} correlates with an chiX angle of ~$\pm$ 75º for the particular Trp residue. For tryptophan in solution and in most proteins, this frequency region typically exhibits a doublet at ~1360 and 1340 cm^{-1}, which arises from the interaction of the W7 mode with several out-of-plane modes (*32*). The intensity ratio I_{1360} / I_{1340} is known to be a measure of the hydrophobicity of the environment of a particular Trp residue. It varies from 0.7-0.9 in hydrophilic solvents to 1-1.1 in benzene and its derivatives and upto 1.2-1.3 in saturated hydrocarbons (*43*).

It is possible to ascribe shifts in vibrational line amplitude to differences in enzymatic activity and not sidechain involvement in DNA repair, but the clear and distinct vibrational frequency shifts between the labeled and unlabeled repair spectrum are unambiguous in this regard. The difficulty is defining the role of the tryptophanyl sidechains in the repair process.

The crystal structures of photolyase enzymes (*44-46*) and molecular modeling of the enzyme bound substrate have shown that there are two tryptophan residues in the immediate vicinity of the proposed docking site, Trp 277 and Trp 384 (*10-13, 47*). There is some disagreement in the literature whether these residues play a structural or a catalytic function. It has been demonstrated previously that perturbations in tryptophan sidechains may be observed when the indole ring system is used to dictate structure (*48*). Perturbation of the indole rings can be monitored in the >800 cm^{-1} region of the spectrum, but these steric interactions did not affect the fingerprint region of the spectrum. In this work ring stacking interactions would not be observed.

Evidence for tryptophan involvement in photorepair has been confirmed from site-directed mutagenesis studies, showing a decrease in repair activity upon substitution

of a phenylalanine at position 384, and almost a complete loss of repair activity when phenylalanine is substituted at position 277 (*6*). It should be noted that phenylalanine substitution at position 277 did not significantly inhibit protein-substrate binding (*7*).

The general reaction mechanism for dimer repair has been described previously (*49*), with the first step being an anion radical formation at the 5' C4=O position. The new oxyanion, proximal to tryptophan 277 in docking studies, would drive the deprotonation of tryptophan to form the neutral radical species. After splitting of the dimer the proton and electron is transferred back to the tryptophan neutral radical, followed by back electron transfer to FADH-, restoring both to ground state.

Evidence has been presented in the literature suggesting that electron donation to the CPD lesion is a one-way process (*50*), but this view is not consistent with quantum yield and turnover values of photorepair (*51*).

Validation for the proposed process lies in mathematical and computational models previously reported (*10-13*). The findings of these experiments are in agreement that the electron transfer from FADH- to the CPD lesion is indirect. They propose that either the adenine ring (*10, 12*) or a tryptophan side chain (*11, 13*) acts as the intermediary, but none have direct evidence. The results from our experiments indicate that tryptophan is involved in this process, but do not exclude involvement of the adenine ring of FAD. This is a topic for future isotope editing experiments.

ACKNOWLEDGEMENTS

Lori McKee is acknowledged for technical assistance in obtaining infrared data on FAD redox changes. We are indebted to Prof. Aziz Sancar (Univ. North Carolina) for providing the photolyase expression vector. We thank Profs. Timothy Larson and E. Mick Gregory (Virginia Tech) for providing advice, support, and plasmids for the tryptophan labeling experiments. Thomas Krick (University of Minnesota Mass Spectrometry Consortium for the Life Sciences) is credited for his mass spectral analysis of isotopomers composition of our protein samples. Prof. Edward Wojcik (Virginia Tech) and Ross Willis were invaluable for their efforts in establishment of the IR and laser systems. This work was supported by American Chemical Society–Petroleum Research Fund (38643-G4 to S.K.), American Cancer Society (IRG-99-225-01 to S.K.), and the Thomas F. and Kate Jeffress Trust (J-613 to S.K.)

REFERENCES

1. Sjoberg, B. M., and Reichard, P. (1977) *J Biol Chem 252*, 536-541.
2. Stubbe, J., and van Der Donk, W. A. (1998) *Chem Rev 98*, 705-762.
3. Jovanovic, S., Steenken, S., and Simic, M. (1991) *J Phys Chem 95*, 684-687.
4. Aubert, C., Mathis, P., Eker, A. P., and Brettel, K. (1999) *Proc Natl Acad Sci U S A 96*, 5423-5427.
5. Aubert, C., Vos, M. H., Mathis, P., Eker, A. P., and Brettel, K. (2000) *Nature 405*, 586-590.
6. Kim, S. T., Li, Y. F., and Sancar, A. (1992) *Proc Natl Acad Sci U S A 89*, 900-904.
7. Li, Y. F., and Sancar, A. (1990) *Biochemistry 29*, 5698-5706.
8. MacFarlane, A. W., and Stanley, R. J. (2003) *Biochemistry 42*, 8558-8568.
9. MacFarlane, A. W., and Stanley, R. J. (2001) *Biochemistry 40*, 15203-15214.
10. Antony, J., Medvedev, D. M., and Stuchebrukhov, A. A. (2000) *J Am Chem Soc 122*, 1057-1065.
11. Hahn, J., Michel-Beyerle, M.-E., and Roesch, N. (1999) *J Phys Chem B 103*, 2001-2007.
12. Medvedev, D., and Stuchebrukhov, A. A. (2001) *J Theor Biol 210*, 237-248.
13. Sanders, D. B., and Wiest, O. (1999) *J Am Chem Soc 121*, 5127-5134.
14. Sancar, A., Smith, F. W., and Sancar, G. B. (1984) *J Biol Chem 259*, 6028-6032.
15. Gindt, Y. M., Vollenbroek, E., Westphal, K., Sackett, H., Sancar, A., and Babcock, G. T. (1999) *Biochemistry 38*, 3857-3866.
16. Li, Y. F., Heelis, P. F., and Sancar, A. (1991) *Biochemistry 30*, 6322-6329.

17. Malhotra, K., Kim, S. T., Walsh, C., and Sancar, A. (1992) *J Biol Chem 267*, 15406-15411.

18. Jorns, M. S., Sancar, G. B., and Sancar, A. (1984) *Biochemistry 23*, 2673-2679.

19. Sancar, A., and Sancar, G. B. (1984) *J Mol Biol 172*, 223-227.

20. Laemmli, U. K. (1970) *Nature 227*, 680-685.

21. Bitner, R. M., and Kuempel, P. L. (1982) *J Bacteriol 149*, 529-533.

22. Waldburger, C., and Susskind, M. M. (1994) *J Mol Biol 235*, 1489-1500.

23. Kim, S. T., Sancar, A., Essenmacher, C., and Babcock, G. T. (1993) *Proc Natl Acad Sci U S A 90*, 8023-8027.

24. Keller, M. D., Selvin, R. C., Claus, W., and Guillard, R. R. L. (1987) *J Phycol 23*, 633-638.

25. Sambrook, J., and Russell, D. W. (2001) pp A2.1, Cold Spring Harbor Laboratory Press, Cold Spring Harbor, New York.

26. Karnaukhova, E., Niessen, W. M., Tjaden, U. R., Raap, J., Lugtenburg, J., and van der Greef, J. (1989) *Anal Biochem 181*, 271-275.

27. Liu, F.-T., and Yang, N. C. (1978) *Biochemistry 17*, 4865-4876.

28. Deering, R. A., and Setlow, R. B. (1963) *Biochim Biophys Acta 68*, 526-534.

29. Jorns, M. S., Sancar, G. B., and Sancar, A. (1985) *Biochemistry 24*, 1856-1861.

30. Mohan, S., Puviarasan, N., and Bakkialakshmi, S. (1999) *Asian J Chem 11*, 1137-1143.

31. Bunte, S., Jensen, G., McNesby, K., Goodin, D., Chabalowski, C., Nieminen, R., Suhai, S., and Jalkanen, K. (2001) *Chem Phys 265*, 13-25.

32. Takeuchi, H., and Harada, I. (1986) *Spectrochim Acta 42*, 1069-1078.

33. Lautie, A., Lautie, M. F., Gruger, A., and Fakhri, S. A. (1980) *Spectrochim Acta 36*, 85-94.

34. Wille, G., Ritter, M., Friedemann, R., Mantele, W., and Hubner, G. (2003) *Biochemistry 42*, 14814-14821.

35. Walden, S. E., and Wheeler, R. A. (1996) *JPhys Chem 100*, 1530-1535.

36. Hoffman, B. M., Roberts, J. E., Kang, C. H., and Margoliash, E. (1981) *J Biol Chem 256*, 6556-6564.

37. Behmoaras, T., Toulme, J. J., and Helene, C. (1981) *Proc Natl Acad Sci U S A 78*, 926-930.

38. Cochran, A. G., Sugasawara, R., and Schultz, P. G. (1988) *J Am Chem Soc 110*, 7888-7890.

39. Chirgadze, Y. N., Fedorov, O. V., and Trushina, N. P. (1975) *Biopolymers 14*, 679-694.

40. Popovic, D. M., Zmiric, A., Zaric, S. D., and Knapp, E. W. (2002) *J Am Chem Soc 124*, 3775-3782.

41. Schmitz, M., Tavan, P., and Nonella, M. (2001) *Chem Phys Lett 349*, 342-348.

42. Miura, R., Nishina, Y., Ohta, M., Tojo, H., Shiga, K., Watari, H., Yamano, T., and Miyake, Y. (1983) *Biochem Biophys Res Comm 111*, 588-594.

43. Miura, T., Takeuchi, H., and Harada, I. (1988) *Biochemistry 27*, 88-94.

44. Tamada, T., Kitadokoro, K., Higuchi, Y., Inaka, K., Yasui, A., de Ruiter, P. E., Eker, A. P., and Miki, K. (1997) *Nat Struct Biol 4*, 887-891.

45. Park, H. W., Kim, S. T., Sancar, A., and Deisenhofer, J. (1995) *Science 268*, 1866-1872.

46. Komori, H., Masui, R., Kuramitsu, S., Yokoyama, S., Shibata, T., Inoue, Y., and Miki, K. (2001) *Proc Natl Acad Sci U S A 98*, 13560-13565.

47. Volcov, F., and Goldman, C. (2004) *J Chem Phys 120*, 3381-3386.

48. Roepe, P., Gray, D., Lugtenburg, J., van den Berg, E., Herzfeld, J., and Rothschild, K. (1988) *J Am Chem Soc 110*, 7223-7224.

49. Heelis, P. F., Kim, S.-T., Okamura, T., and Sancar, A. (1993) *J Photochem Photobiol B 17*, 219-228.

50. Ma, L., Li, J., Qu, L., Hager, J., Chen, Z., Zhao, H., and Deng, X. W. (2001) *Plant Cell 13*, 2589-2607.

51. Kavakli, I., and Sancar, A. (2004) *Biochemistry 43*, 15103-15110.

SUMMARY AND OUTLOOK

The first objective of this thesis was to elucidate the chemical bonds and structural features indicating the presence of a cyclobutane pyrimidine dimer in oligonucleotides. This was accomplished using difference FT-IR spectroscopy to compare oligomer DNA in the presence and absence of the CPD lesion, and in the presence and absence of methyl groups at the C5 position of the pyrimidine ring. Distinct shifts are observable in the vibrational spectrum related to the stretching modes of the phosphodiester backbone, carbonyl stretching, and fundamental C-H stretching.

The chemical bonds that form the CPD ring were not detected directly. We believe that the vibrational lines directly indicative of the cyclobutane ring may be obscured by the high absorbance of the phosphate stretching modes. Further CPD studies would involve isotopic labeling of the C5 and C6 positions; comparison with non-labeled CPD oligonucleotides would reveal the positions of these shifted modes upon creation of difference spectra. The chemical bonds that form the CPD lesion do influence the stretching modes of the pyrimidine carbonyls, which act as an indirect marker for the formation of the cyclobutane pyrimidine dimer.

Novel to this thesis is description of the high frequency region of the vibrational spectrum of DNA in order to ascribe changes in bonding and structure of the oligonucleotide. Usually limited to demarking the presence of chemical groups and DNA bases, the high frequency region of the vibrational spectrum has shown clear and distinct shifts of the C5 methyl and C6-H atom groups upon modification of an oligonucleotide. Although subtle changes in this region have been reported for DNA from different tissues

and cancerous tumors, the utility of this information is limited because the explanation for the vibrational shifts was left undefined.

We have described definitive evidence for DNA structural changes, seen in the shift of the frequencies indicative of the phosphodiester backbone. Although conformational description of single-stranded oligonucleotides is under debate in the literature, the ability to detect a single, non-uniform phosphate stretching mode has been described. This may be of utility in studies of cancer therapy drugs or in the study of DNA damage of other forms. Future work in this area would be focused on developing a library of "normal" and specifically altered DNA spectra for comparison to clinical samples.

The second objective of this thesis was to determine if tryptophan is a participant in the electron transfer event that leads to DNA repair by photolyase. Using a combination of difference FT-IR techniques and isotopic labeling, we have determined that tryptophan does play a role in the repair reaction, forming radical species as an electron transfer intermediate. This work stands in direct contrast to approximately half of the published studies on photolyase-catalyzed photorepair. Future work will be focused on determining the exact identity of the tryptophan residue involved in photorepair, and maximization of signal by performing the experiments at lower temperatures.

A novel finding of this work was the possible interaction of the amino acid sidechain with the peptide backbone. Although spin delocalization from the indole ring to the peptide backbone has been suggested in tryptophan, this is the first evidence of the phenomenon being observed. Review of the literature in association with this thesis has

revealed a paucity of information on the tryptophan radicals. There is a definite need for the elucidation of tryptophan radical vibrational spectra, but also an understanding of the electronic structure of the radicals. This work will require a combined FT-IR, EPR, and possibly NMR, research regimen to fully comprehend the function of tryptophan as an electron transfer hub.

Another branch of the photolyase / photorepair work will be to focus on the role of the adenine moiety of FAD in the photorepair process. Using similar techniques for isotopic replacement used for tryptophan labeling, the adenine moiety could be specifically labeled and studied by difference FT-IR. Since the majority of photorepair studies indicate a role for the adenine ring, these experiments would experimentally define the role, which may provide the first evidence of adenine-facilitated electron transfer.

VITA

Eldon Kenneth Hurley Jr.
Department of Biochemistry
Virginia Polytechnic Institute and State University
Blacksburg, VA 24061
Email address: ekhurley@vt.edu, ekhurley@yahoo.com

Personal History

Born in Carthage, MO on June 15th, 1974

Education

Pulaski County High School, Dublin, Virginia, Sept. 1988-June 1992

B.S., Psychology, Virginia Polytechnic Institute and State University, Blacksburg, Virginia, Aug. 1992-Dec. 1997

B.A., Chemistry, Virginia Polytechnic Institute and State University, Blacksburg, Virginia, Aug. 1998-May 2002

Professional Experience

Employer: Mountain Lake Hotel, A. C. Porterfield
Type of Employment: Laboratory Technician / Assistant Supervisor
Inclusive Dates: Jun. 1995-July 1998

Employer: Virginia Polytechnic Institute and State University, Prof. W.H. Velander
Type of Employment: Laboratory Technician
Inclusive Dates: Jan. 1999-Sept. 1999

Employer: Virginia Polytechnic Institute and State University, Prof. S. Kim
Type of Employment: Laboratory Technician
Inclusive Dates: Dec. 2000-May 2002

Memberships

Member, Triangle Fraternity 1993-Present
Member, Biophysical Society 2004-Present

Awards

Recipient of James F. Eheart Travel Scholarship, 2003
Recipient of Va. Tech GSA Poster Presentation Award, 2004

Presentations

GSA Poster Competition, 2003
Biophysical Society National Meeting, 2004
GSA Poster Competition, 2004